IS-T- 386

AMES LABORATORY

Iowa State University

Ames, Iowa

AEC Contract No. W-7405-eng-82

MEASUREMENT OF TURBULENT DIFFUSION AT SHORT OBSERVATION TIMES USING SPIN-ECHO NMR

by

Marlyn Jerome Murtha

M.S. Thesis, May 1970

DISCLAIMER

This report was prepared as an account of work sponsored by an agency of the United States Government. Neither the United States Government nor any agency Thereof, nor any of their employees, makes any warranty, express or implied, or assumes any legal liability or responsibility for the accuracy, completeness, or usefulness of any information, apparatus, product, or process disclosed, or represents that its use would not infringe privately owned rights. Reference herein to any specific commercial product, process, or service by trade name, trademark, manufacturer, or otherwise does not necessarily constitute or imply its endorsement, recommendation, or favoring by the United States Government or any agency thereof. The views and opinions of authors expressed herein do not necessarily state or reflect those of the United States Government or any agency thereof.

DISCLAIMER

Portions of this document may be illegible in electronic image products. Images are produced from the best available original document.

MEASUREMENT OF TURBULENT DIFFUSION

AT SHORT OBSERVATION TIMES

USING SPIN-ECHO NMR

by

Marlyn Jerome Murtha

A Thesis Submitted to the

Graduate Faculty in Partial Fulfillment of

The Requirements for the Degree of

MASTER OF SCIENCE

Major Subject: Chemical Engineering

Approved:

In Charge of Major Work

Head of Major Department

Dean of Graduate College

Iowa State University
Ames, Iowa

1970

Abstract

A flow observation technique based on spin-echo nuclear magnetic resonance (NMR) has been used to obtain statistical volumetric data of eddy motion in turbulent flow. The NMR procedure, using 90°-180° Carr-Purcell pulses, was particularly adapted to flow observation over very short times. This provided Lagrangian turbulence data for the initial phase of the correlation decay. The technique used to obtain the data is described.

TABLE OF CONTENTS

INTRODUCTION

A more thorough understanding of turbulence of a fluid in a pipe or other duct geometry is of interest because of the wide range of industrial processes which turbulent motion affects. The basic phenomena of heat and mass transfer are greatly affected by turbulence in the system. With practical application in the optimal design of refining, absorption, and chemical reaction equipment, there is a great incentive to obtain a better understanding of turbulence. Although much research has been done on the study of turbulence the complexity of the subject has made it difficult to obtain valid direct measurements. Data have been collected in the form of concentration profiles or by using some type of an anemometer. With these techniques it has been shown that the fluid flow is influenced by the measuring device, which must be located in the fluid. This type of investigation yields data, taken over relatively long periods of time, but cannot provide information at the very short times when the turbulent effects are most rapidly changing.

This research employed the natural phenomenon of spin-echo nuclear magnetic resonance (NMR) to detect molecular motion in a flowing fluid sample. The spin-echo technique has been used to measure molecular diffusion coefficients of several liquids, but modifications were required to

adapt the technique to a highly turbulent sample. Spin-echo NMR can be used to study the system without physically affecting flow, and the data can be interpreted as a statistical "snapshot" of the position of the particles at a particular instant in time. The technique provides several advantages over more conventional measurement techniques. No foreign object or material, of substantial quantity, need be added to the system to follow the motion of the molecules. The principle of spin-echo nuclear magnetic resonance is based on the orientation of the nuclear magnetic moment vectors of the system. The only outside effect on the system is the magnetization of some of the system components.

Turbulence measurements are generally made in an Eulerian frame (stationary observer) where instantaneous velocity fluctuations separated by some distance are recorded. More meaningful results could be obtained by using a Lagrangian frame of reference (observer moving with the fluid) because the mixing properties of a turbulent fluid are closely related to, and may be predicted from, Lagrangian turbulence parameters. Spin-echo NMR provides Lagrangian measurements directly.

Turbulence can be characterized by two parameters-- intensity (eddy velocity) and scale (eddy lifetime). When considering isotropic turbulence, the parameters represent

average volumetric values. Isotropic turbulence is described by Brodkey (7) as homogeneous, implying that the velocity fluctuations in the system are random and that the average turbulent characteristics are independent of position in the fluid. In addition, the velocity fluctuations are independent of the axes of reference, and invariant to axis rotation or reflection.

Statistical theory of turbulence has predicted that turbulent motion is a function of time and not a constant as assumed in molecular diffusion work. Several attempts have been made to characterize or correlate turbulence as a function of time and a time dependence has been shown. No data have been obtained at very short diffusion times, or by use of a sensitive direct measurement technique as used in this work. Spin-echo NMR has the advantage of observing motion over very short diffusion times, and the disadvantage that it is presently limited to short diffusion times or low flow rates. However, for the observation times from 4 msec to 10 msec, and a flow range 3,000 to 7,000 Reynolds' number, this research demonstrates that very sensitive measurements of turbulent motion can be made, and that a significant time dependence is evident.

PREVIOUS WORK

An introductory discussion of the study of fluid tur-
bulence may be found in chemical engineering texts such as
those by Knudsen and Katz (23), Sherwood and Pigford (37),
and Bird et al. (5). More detailed treatments of turbulence
are contained in such texts as Hinze (21), Batchelor (4),
and Brodkey (7). The book by Hinze contains an extensive
treatment of the mechanisms and theories of turbulence, with
reviews of measurement techniques and transport processes.
Information on nonisotropic turbulence is presented.
Batchelor provides a thorough discussion of the subject of
homogeneous turbulence. The theoretical aspects of homoge-
neous turbulence are emphasized, and experimental data are
presented to substantiate the various theories.

The development of the statistical theory of turbulence
is based on mathematical derivations by G. I. Taylor (40,41,
42). His classical work provides the basis of turbulence
research and will be discussed in detail in a later section.

Turbulent diffusion was studied by Hanratty, Latinen,
and Wilhelm (20). Measurement of the spreading of tracer
dye from a point source yielded information on diffusion
in glass-sphere beds fluidized by water. A particulately
fluidized bed was well described by the statistical turbu-
lence equations of Taylor. Experimental data confirmed
the theory that turbulent measurements were within a

turbulent "mean free path" or scale. As a result, for diffusion from a fixed-point source, the size of the turbulent diffusion coefficient depended on the time of diffusion. The diffusion coefficient became constant only after a long time interval had elapsed in a given experiment.

Hanratty (19) used the information derived from the statistical analysis of turbulence to show that, for turbulent transport processes the mixing depends on the previous history of the diffusing material. The effect of time on the diffusion process was examined for the case of heat transfer from a hot wall to a cold wall through a turbulently flowing liquid. G. I. Taylor's theory of turbulent diffusion for an isotropic field was used to describe the properties of the heat sources and cold sinks along the walls. These calculations were compared with temperature profiles obtained as a solution to Fick's law using a constant diffusion coefficient. A marked difference between these profiles was shown; then a comparison with actual temperature measurements verified the time dependency.

Flint et al. (13) studied turbulent diffusion from a point source located at the center of the tube. The Lagrangian intensity of the turbulence in the center of the tube was calculated from the diffusion data. The

relative longitudinal intensity, the ratio of the square root of the intensity to the average velocity at the center of the tube, varied from 0.058 at N_{Re} = 9,700 to 0.039 at N_{Re} = 83,000. The results could not be used for determining the form of the correlation coefficient because of inaccuracies in the measurements at small diffusion times. Both air and water flow in 3-inch dia. smooth pipe was used to obtain the diffusion data. The diffusion coefficients and mean square displacements were calculated from concentration profile measurements, and the results were somewhat higher than values obtained from hot-wire studies. The difference might be explained by the disturbances created by the tracer injector. Mickelson (26), using a carefully designed injection system in a much larger diameter pipe, obtained turbulent intensities in close agreement with those measured with a hot-wire anemometer.

Sandborn (33) measured longitudinal and radial intensities for air flowing in a 4-inch dia. pipe using hot-wire anemometry methods. Data were obtained over the Reynolds' number range 20,000 to 200,000. Relative longitudinal intensities were slightly higher than comparable radial intensities, but both decreased slightly as Reynolds' number increased. Relative longitudinal intensities at the center of the tube were 0.034 at 20,000 Reynolds' number and 0.025 at 170,000 Reynolds' number.

The relative radial intensities were 0.025 at 50,000 Reynolds' number and 0.023 at 170,000 Reynolds' number, quite constant. Sandborn also measured relative radial intensity profiles across the tube. These profiles showed that the average intensity was higher than that measured at the center of the tube.

Air turbulence in a 5-inch square channel was investigated by Laufer (24) using a hot-wire anemometer. In a lower Reynolds' number range, $12,000 < N_{Re} < 62,000$, the relative longitudinal intensity at the center of the channel decreased from 0.032 to 0.027 and the relative radial intensity changed from 0.025 to 0.021.

Seagrave (35) studied mass transfer in turbulent liquid streams using water as the bulk fluid. Dye was injected into a water stream and samples were taken at a distance far enough downstream so that the eddy diffusivity had become constant. The concentration of dye in each sample was determined colorimetrically. Average radial and axial eddy diffusivity components were reported. Variation of the average radial diffusivity was linear with Reynolds' number over the range 3,000 to 7,500.

Grossman and Charwat (17) measured longitudinal and radial turbulent intensities for water flow in a 2-inch dia. pipe using a method based on electromagnetic induction. The technique offered advantages in sensitivity over the

hot-wire anemometer and concentration measurement methods but still required entering the system with probes, and suffered from a poor signal to noise ratio. At a Reynolds' number of 99,000, relative radial and longitudinal intensities of 0.013 and 0.017 respectively were measured at the center of the tube. Examination of intensity profiles showed that the average relative longitudinal intensity was about 0.018 and the radial value was 0.011 for that Reynolds' number. These profiles showed maximum radial intensity at the center of the tube.

Martin and Johanson (25) used a hot-film anemometer to measure the Eulerian longitudinal intensity and time scale of turbulence in the center of a tube for a flowing water system. Intensity, scale, and correlation coefficients were obtained for velocities ranging from 0.5 to 4.0 ft/ sec (N_{Re} = 19,000 to 160,000). The Eulerian parameters were calculated from measurements taken from photographs of the oscilloscope traces. These data were presented as correlation versus time over the velocity range. The time scale of turbulence, the integral of the correlation curve, decreased with increasing Reynolds' number from 40 msec at a Reynolds' number of 19,000 to 12 msec at a Reynolds' number of 160,000.

Longitudinal turbulent intensities, autocorrelations and energy spectra were measured using several organic

solvents by Patterson and Zakin (29). The flow of toluene, benzene, and cyclohexane in smooth 1 and 2-inch dia. tubes was studied using a constant temperature, hot-film anemometer. Relative longitudinal intensity profiles showed that the maximum values occurred at a distance about 15 percent of the pipe radius away from the wall, and were about two and one-half times higher than the value measured at the center. Eulerian length scales of turbulence were calculated for the three fluids of different viscosities. No viscosity effect was noted for the different solvents. An estimate of the overall average longitudinal intensity across the tube from a partial intensity profile was about 50 percent higher than the intensity at the center of the tube.

Most of the results from this previous work has provided Eulerian information (stationary observer). Parameters obtained by the Lagrangian method (observer moves with the fluid) would provide information more directly related to the mixing properties of the fluid but Lagrangian measurement techniques were not available. The utilization of spin-echo NMR phenomena as a measurement technique provides a Lagrangian technique for investigating flowing systems. Research using spin-echo NMR on dynamic samples was conducted by Arnold (3). Information on the effect of a velocity profile on the NMR signal was obtained.

Johnson (22) extended this study, measuring apparent radial diffusivities for water flowing in a tube. The results were termed apparent because the NMR procedure determines total movement in a direction parallel to the magnetic field rather than in a radial direction. The NMR data were then corrected to estimate a radial diffusivity. These diffusivity values increased linearly with Reynolds' number over the range, $1,060 < N_{Re} < 6,760$. Diffusivities significantly higher than the molecular diffusion constant were obtained for Reynolds' numbers as low as 1,060.

Conway (11) used spin-echo NMR to measure average unidirectional diffusivities for water flow in the range, $220 < N_{Re} < 3,740$, at a single diffusion time. This research provided a careful study of turbulent motion in the transition flow range.

Several other new nondestructive techniques have been developed for study of fluid flow. Some are specific to flow at the walls, while others can provide profile data.

Reiss and Hanratty (31, 32) used an electrochemical technique analogous to the constant temperature, hot-wire anemometer measurement. The concentration of the diffusing species was constant at the electrode surface and the current was proportional to the rate of mass transfer to the electrode. Velocities in the region close to the wall were measured using a diffusion controlled electrode mounted

flush with the wall. The test electrode formed part of an electrochemical cell.

An electrochemical cell using an aqueous solution of potassium ferri- and ferrocyanide with nickel electrodes was used by Gordon and Tobias (16) for the measurement of diffusion coefficients for the ferricyanide ion. The electrochemical technique has been extended by Mitchell and Hanratty (27) and the relation between mass transfer measurements and the velocity field was defined more accurately. By measuring the limiting current at an electrode at $12\text{-}1/2^{\circ}$ to 20° as well as perpendicular to the flow, Sirkar and Hanratty (38) measured the root-mean-squared transverse component of the turbulent velocity fluctuations close to the wall.

Capps and Rehm (8) have developed an empirical expression based on the experimental data of Nikuradse for the turbulent flow velocity distribution. This relationship, which predicted data over a Reynolds' number range from 9,000 to 3,000,000, had surface roughness as the primary parameter. Eddy diffusivity profiles across the tube were given at several Reynolds' numbers. These curves showed a maximum value at a distance equal about 40 percent of the radius from the wall.

A study of turbulent mixing was done by Christiansen (10). Studies of turbulent motion and turbulent mixing are

very similar, with the simplification that dependent
variables, position, velocity, which are vectorial in the
study of turbulent motion can be replaced by scalar quan-
tities, composition, dielectric constant, and temperature.
This work presents a technique for obtaining direct tur-
bulence data. Time-average light-scatter measurements using
a laser generated light gave directly the spectrum for
spatial variations in concentration. The concentration
spectrum is a Fourier transform of the concentration corre-
lation, $R(r,t)$. Spatial resolution of light scatter was
100 times better than the smallest probe used to date, and
this is a nondestructive technique which will not disturb
local motion.

Another related technique for turbulent flow measure-
ments was used by Goldstein and Hagen (15). The Doppler
shift of scattered light from a laser beam was used to
measure mean turbulence velocities, and also to determine
the probability function for the turbulent velocity. A
phenomenon which is evident by NMR methods was noted. As
flow went through the transition from laminar to turbulent,
the signal was irregular and erratic. As flow became fully
turbulent the signal become steady again. Relative longi-
tudinal intensities were measured, and these agreed well
with an extrapolation of the data of Laufer (24). The
relative longitudinal intensities decreased from 0.042 at

5,000 Reynolds' number to 0.035 at 20,000 Reynold's number.
This technique presents some unique advantages. As in NMR
no probe interferes with flow, and the velocity component
in a single direction can be measured. In addition, local
measurements would be possible.

A nondisturbing tracer technique for turbulent flow
observation was used by Frantisak et al. (14). A photochromic
dye was dissolved in the test fluid and irradiated with
ultraviolet light to produce a colored trace, allowing
quantitative measurements in the entire cross section of
the tube in both laminar and turbulent flow. A ruby laser
was used to induce the tautomeric reaction in the dye, and
quantitative measurements were made from high speed movies.
Mean velocity profiles were measured, and mean shear stresses
at the wall were calculated over a range of Reynolds' numbers.
There was excellent agreement with other, well established
data.

DIFFUSION IN ISOTROPIC TURBULENCE

Turbulence has been defined by Taylor and Von Karman (43) as an irregular motion which in general makes its appearance in fluids, gaseous or liquid, when they flow past solid surfaces or even when neighboring streams of the same fluid flow past or over one another. These irregular motions will prevail even at steady state if the flow system is turbulent. Because the motion is irregular it is not possible to describe the motion in all detail as a function of time and space coordinates. But the type of irregularity is such that turbulent motion can be described by laws of probability. Therefore, turbulence is a special type of irregular motion showing random variation with time and space coordinates, but statistically distinct average values of the fluctuations can be discerned.

When the turbulence has the same characterization at all points in the flow field it is referred to as homogeneous turbulence. If the statistical parameters of turbulence have no preferred direction the turbulence is said to be isotropic. Therefore, isotropic turbulence is a distinct type of homogeneous turbulence.

Isotropic turbulence is the least complex state of turbulence to analyze because a minimum number of properties are required to characterize its structure and behavior. It is a hypothetical type of turbulence in that no actual flow

is completely isotropic. Such turbulence can be approached in flow with a high pressure drop and improved by placing a grid network across the flow stream. Because of its simplicity isotropic flow is often assumed at least as a first approximation, but with the information which is available about turbulent motion this assumption represents a small error when compared with other unknowns.

The development of the statistical theory of turbulence, by Taylor (40,41,42) for diffusion in isotropic turbulence will be summarized since this has been the basis for modern turbulence research.

An isotropic turbulent field is assumed with a number of fluid particles starting from different positions at the same time. With the simplest assumption, that of diffusion in only one direction, motion perpendicular to the flow will be described. The fluid is flowing in the z direction and motion in the y direction will be followed. If the turbulent velocity of a single particle in the y direction is $v(t)$, the displacement of the particle after a time t is

$$Y(t) = \int_0^t v(t)\, dt \qquad (1)$$

Since $v(t)$ is a random quantity, the average for a large number of particles, $\overline{Y}(t) = 0$. However, the mean-square displacement will not be zero. For homogeneous flow, the mean-square displacement in the y direction is given by

$$\overline{Y^2}(t) = \int_0^t dt_2 \int_0^t dt_1 \ \overline{v(t_1) \ v(t_2)} \tag{2}$$

where $v(t_1)$ is the velocity of the particle when $t = 0$ and $v(t_2)$ is the velocity at $t = t$. The integration in the (t_1, t_2) plane is over a square with limits 0 and t. To simplify, instead of this square, integrate over twice the triangle formed by the half square, since the integrand is symmetrical with respect to t_1 and t_2. This gives

$$\overline{Y^2}(t) = 2\int_0^t dt_1 \int_0^{t_1} dt_2 \ \overline{v(t_1) \ v(t_2)} \tag{3}$$

The velocities at the two instances for short times are not independent, they are correlated by the Lagrangian correlation coefficient defined as

$$R(t_1, t_2) = \frac{\overline{v(t_1) \ v(t_2)}}{\overline{v^2}} \tag{4}$$

where $\overline{v^2}$ is the mean-square turbulent velocity. To intro-duce $R(t_1, t_2)$ into Equation 3, $\overline{v(t_1) \ v(t_2)}$ can be a function of time change rather than absolute time since flow is steady, then

$$R(s) = \frac{\overline{v(t_1) \ v(t_1 + s)}}{\overline{v^2}} \tag{5}$$

where $s = t_2 - t_1$. Substituting

$$\overline{Y}^2(t) \;=\; 2 \int_0^t dt_1 \int_0^{t_1} dt_2 \; \overline{v}^2 \, R(s) \tag{6}$$

or

$$\overline{Y}^2(t) \;=\; 2 \, \overline{v}^2 \int_0^t dt_1 \int_0^{t_1} R(s)\,ds \tag{7}$$

The correlation coefficient can be defined for continuous diffusion as

$$R(s) \;=\; 1 - \frac{s^2}{2!} \frac{\left[\dfrac{d\overline{v}}{dt}\right]^2}{\overline{v}^2} + \frac{s^4}{4!} \frac{\left[\dfrac{d^2\overline{v}}{dt^2}\right]^2}{\overline{v}^2} - \cdots$$

$$+ \frac{(-1)^n \, s^{2n} \left[\dfrac{d^n\overline{v}}{dt^n}\right]^2}{2n!\,\overline{v}^2} \tag{8}$$

It can be shown that $R(s)$ is an even function. Then integrating Equation 7 by parts yields

$$\overline{Y}^2(t) \;=\; 2\overline{v}^2 \, t \int_0^t R(s)\,ds \;-\; \int_0^t s R(s)\,ds$$

$$=\; 2\overline{v}^2 \int_0^t (t - s) \, R(s)\,ds \tag{9}$$

This relationship defines the time dependence of turbulent motion.

The variation of $\overline{Y}^2$ with time for molecular diffusion from a fixed point can be shown to be

$$D = \frac{\overline{Y}^2}{2t} = \text{constant} \qquad (10)$$

where D is the molecular diffusivity. Systems involving molecular diffusion are described by Fick's law using appropriate boundary conditions as

$$\frac{dC}{dt} = \nabla \cdot (D\nabla c) \qquad (11)$$

which involves the assumption that the diffusion characteristics of particles contained in a differential volume are not dependent on the previous history of the particle. This independence is not present in turbulent diffusion since $\overline{Y}^2/2t$ is a function of time. Hanratty (19) derives the relationships for solving a modified Fick's law equation. This yields a turbulent diffusivity, E(t), defined as

$$E(t) = \frac{\overline{Y}^2(t)}{2t} \qquad (12)$$

where E will vary with time.

If a shape for the correlation coefficient is assumed, then $\overline{Y}^2$ can be calculated as a function of time. As observation time approaches zero, the correlation coefficient approaches unity, and Equation 9 integrates to

$$\overline{Y}^2 = \overline{v}^2 t^2 \qquad (13)$$

For longer times, several assumptions have been pro-

posed. If one assumes that the correlation decays expo-
nentially, then

$$R(s) = e^{-as}$$

and from the definition of Lagrangian scale,

$$T_L = \int_0^\infty e^{-as} \, ds \tag{14}$$

or

$$a = \frac{1}{T_L}$$

Substituting into Equation 9

$$\overline{Y^2}(t) = 2\overline{v^2} \int_0^t (t - s) \, e^{-\frac{s}{T_L}} \, ds \tag{15}$$

which integrates to

$$\overline{Y^2}(t) = 2\overline{v^2} \, T_L \, [t + T_L \, (e^{-\frac{t}{T_L}} - 1)] \tag{16}$$

Only at long time, $t > 10 \, T_L$ does $\overline{Y^2}(t)$ reach a constant
slope where $E = \overline{Y^2}(t)/2t$ is constant. At intermediate
times

$$E(t) = \overline{v^2} \, T_L \, [1 + \frac{T_L}{t} \, (e^{-\frac{t}{T_L}} - 1)] \tag{17}$$

At very long diffusion times this becomes

$$E(t) = \overline{v^2} \, T_L \tag{18}$$

A similar treatment can be made if we assume a correlation decay

$$R(s) = e^{-as^2}$$

then

$$T_L = \int_0^\infty e^{-as^2} ds = \left[\frac{\pi}{4a}\right]^{1/2} \qquad (19)$$

and Equation 9 becomes

$$\overline{Y^2}(t) = 2\overline{v^2} \int_0^t (t - s) e^{-\frac{\pi s^2}{4T_L^2}} ds \qquad (20)$$

This integrates to

$$\overline{Y^2}(t) = 2\overline{v^2} T_L \left[t \, \text{erf}\left(\frac{\sqrt{\pi}t}{2T_L}\right) + \frac{2T_L}{\pi} \left(e^{-\frac{\pi t^2}{4T_L^2}} - 1\right)\right] \qquad (21)$$

and

$$E(t) = \overline{v^2} T_L \left[\text{erf}\left(\frac{\sqrt{\pi}t}{2T_L}\right) + \frac{2T_L}{\pi t} \left(e^{-\frac{\pi t^2}{4T_L^2}} - 1\right)\right] \qquad (22)$$

at long times this assumption also yields

$$E(t) = \overline{v^2} T_L = \text{constant} \qquad (23)$$

These equations represent proposed relationships for diffusion as a function of time. Relative accuracy of the

equations is unknown because they only differ at very short diffusion times, and valid data in that time range have not been available.

SPIN-ECHO NMR

Basic Concepts of NMR

The magnetic properties of the nucleus have been of interest ever since they were first postulated to explain the hyperfine structure of spectral lines. It was supposed that the nucleus is a small magnet whose interaction with the atomic electrons splits the energy levels between which the electrons make the transitions responsible for atomic line spectra. Then, in addition to its known properties of mass, charge, and intrinsic angular momentum, the atomic nucleus possesses a magnetic moment. The nuclei behave as tiny magnets with properties of a gyroscope. The observation of the nuclear magnetic resonance phenomenon is based on the magnetic moment properties of the nuclei.

In this research, hydrogen nuclei, which possess angular momentum and magnetic moments, in water were observed. Not all nuclei possess an angular momentum and a magnetic moment. Purcell (30) gives a general rule to determine if a given nucleus has these properties.

> "If a nucleus contains an even number of protons and an even number of neutrons, it will have zero angular momentum and magnetic moment."

When placed in a strong magnetic field, $\overline{H}_0$, the magnetic moment of spinning hydrogen nuclei tend to align with the direction of the magnetic field. Because the nuclei experi-

ence a resultant torque, the moments will precess about the direction of the applied field. A precessing moment forms a cone of rotation about the direction of the applied field. The frequency of precession, ω_0, is directly related to the magnetic field, $\overline{H}_0$, as

$$\omega_0 = \gamma \, \overline{H}_0 \tag{24}$$

where γ, the gyromagnetic ratio, is defined as the ratio of the magnetic moment to the nuclear angular momentum of the nucleus.

The hydrogen nucleus can exist at two distinct energy levels. In a strong magnetic field the high energy nuclei will precess in one direction and the low energy nuclei will precess in the opposite direction. Since precession frequency is directly related to the force of the magnetic field, this field determines the energy change between these levels. This energy difference, proportional to ω_0, is much less than the force available by thermal vibrations. Therefore, even in a magnetic field there is nearly an equal probability for nuclei in each energy level.

To produce a net magnetic moment it is necessary to create a population imbalance. If the magnetic nuclei can transfer energy to, and come into thermal equilibrium with the surroundings, the equilibrium will favor the lower energy level. This imbalance, which is given by the Boltzmann

factor, exp (-hω/kT), is very minute. For example, if ω = 40 MC/sec and T = 300° K, the factor is 0.9999934. It is on this fractionally minute surplus of nuclei in the lower state at thermal equilibrium that the observable NMR effects depend. Operation at lower temperature will increase this surplus.

The energy change between levels, being proportional to the Larmor frequency, is of radio-wave frequency. Therefore, the radiation of a radio wave or, since the magnetic field of the wave is the effective component, an oscillating magnetic field of radio-wave frequency will excite the nuclei. When the nuclei are subjected to such radiation there is again an equal probability of transitions in either direction. A new population distribution results.

A radio frequency (rf) current passed through a short coil wound axially around a cylindrical tube in which a water sample is placed will generate the rf magnetic field, $\overline{H}_1$, perpendicular to field $\overline{H}_0$ in Figure 1. This force changes the direction of the field and as the nuclei align with this new direction because of the resultant torque, the energy absorbed by the nuclei with the change of direction produces an increase in the number of nuclei in the higher energy level. As the moment direction changes the direction of the torque also changes. This results in the moment being pulled away from the $\overline{H}_0$ direction. This moment
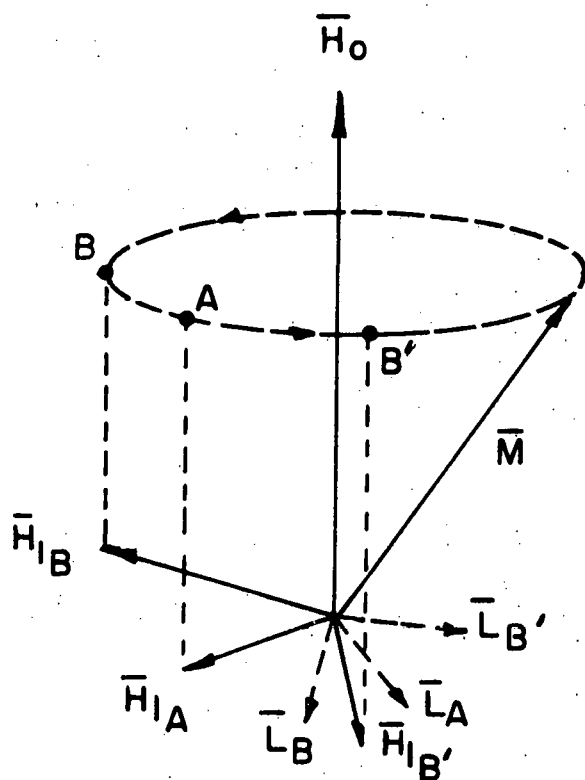
Figure 1.   Change in torque direction if rf field is not
near Larmor frequency

motion while the rf pulse is being applied is called nutation.

If the frequency of the rf current is the same as the frequency of nuclear precession than all the nuclei will be rotated by torque $\bar{L}$ in a fixed direction. This is illustrated on Figure 1, where the magnetic moment $\bar{M}$ rotates at frequency ω_0 around the field $\bar{H}_0$. When the rf pulse is of frequency ω_0 it occurs at a fixed position A with respect to $\bar{M}$, and each nucleus will be rotated away from $\bar{H}_0$. The initial instantaneous torque is $\bar{L}_A$ which tips the moment perpendicular to the plane of $\bar{H}_0 - \bar{H}_{1_A}$. If the rf pulse is at any frequency other than ω_0 the nuclei will be nutated at different points during rotation, i.e., at B then B'. This means that the direction of nutation of the nuclei is constantly changing because of an ever changing torque direction, and the summation of the moment nutation will be zero. The frequency ω_0 at which the magnetic nuclei precess is called the Larmor frequency and the magnetic resonance phenomenon, the resultant moment of the nuclei in the higher energy state, occurs only when the rf current is at the Larmor frequency.

The theory of NMR is dealt with in great detail in books by Andrew (2) and Abragam (1), and in such papers as those by Pake (28), Purcell (30), and Bloch (6).

Generation of the Spin-Echo

The pulsed NMR method known as the spin-echo technique
was developed by Hahn (18) in 1950 and later modified by
Carr and Purcell (9). For the technique, as modified by
Carr and Purcell, rf radiation is applied to a sample in
two bursts, the first is called the 90° pulse and the
second the 180° pulse. The sequence leading to the spin-
echo is illustrated in Figure 2.

When a sample containing hydrogen nuclei is placed in a
strong magnetic field, a net magnetization vector in the
direction of the magnetic field is generated (Figure 2a).
This net magnetization vector consists of a component of
each nucleus in the direction of the applied field summed
over all of the nuclei within the volume of the coil. When
a rf pulse at the Larmor frequency is applied through the
axial coil a magnetic field, $\bar{H}_1$, is created. This field
is oriented perpendicular to the strong magnetic field.
The change in field direction causes a torque on the nuclei
which results in the transition of nuclei to the higher
energy state and moment nutation. The length of time that
the rf current of constant voltage is applied determines
the angle, perpendicular to the x-z plane, through which
the net magnetization vector is rotated. A pulse of proper
length to tip the magnetization vector through 90°, into
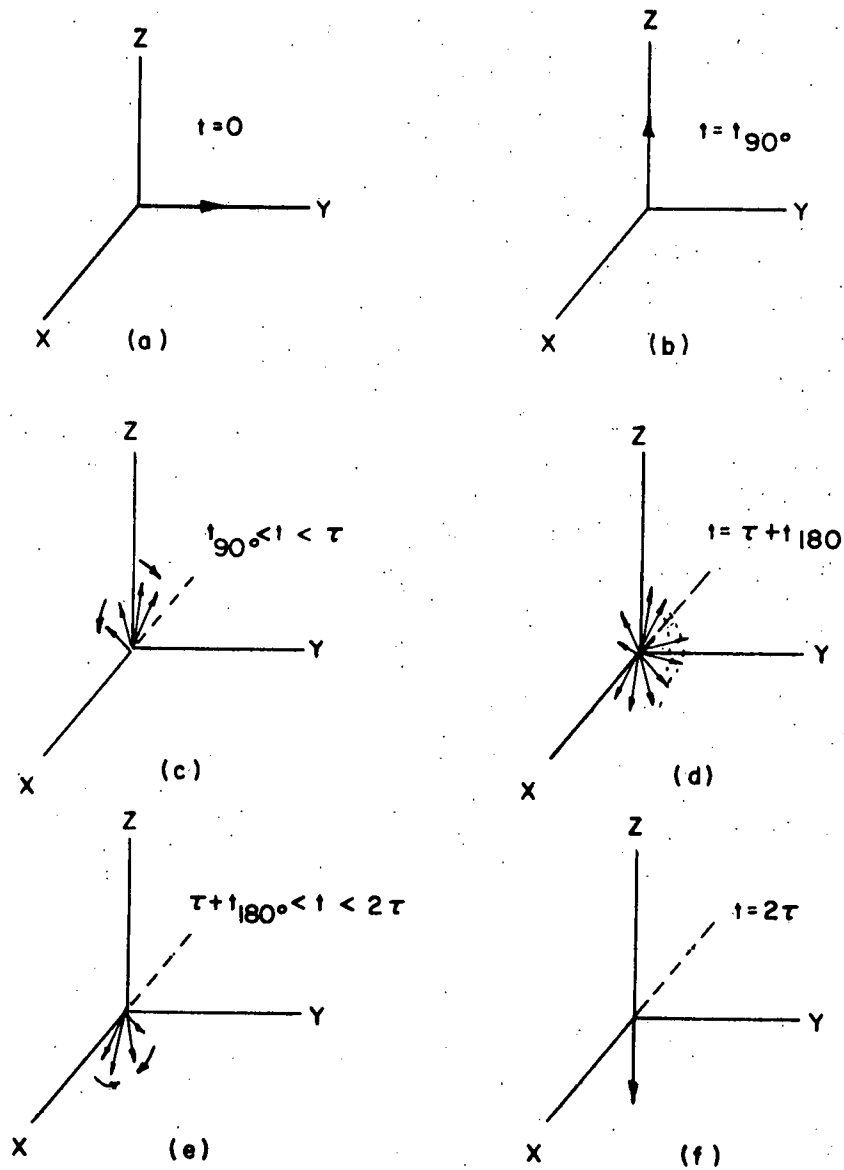the x-z plane, is applied (Figure 2b).

Figure 2. Sequence of moment nutation and precession which generates the spin-echo, as observed in the rotating system

After this length of time the rf pulse is removed and
the magnetization vector precesses about the static field,
$\overline{H}_0$. The lines of force of the precessing net moment cut
the coils of the axial coil and the induced voltage is picked
up by that coil. When the net moment is rotated precisely
into the x-z plane the length of the x-z component is a
maximum and the induced voltage is greatest. The free
precession signal begins to decay immediately.

The nuclei tend to return to their equilibrium, lower
energy state, by a first order decay with time constant T_1.
As nuclei return to the lower energy level they align with
$\overline{H}_0$ which decreases the magnitude of the net x-z component.
The time constant of the return to equilibrium, T_1, is
called the spin-lattice relaxation time because the
released energy is exchanged between the system of nuclear
magnets and the lattice of vibrating atoms.

The precessing nuclei making up the magnetization
vector lose phase coherence because of energy interchanges
within the spin system. The vector loses phase coherence
by a time constant T_2, the spin-spin relaxation time. The
spin-spin decay results because each individual precessing
nuclear moment interacts with neighboring spins through
their magnetic fields. The total magnetic field of any
single nucleus consists not only of the applied field $\overline{H}_0$,
but includes also the resultant of the static components

of neighboring magnetic dipoles. The spread in the applied field due to neighboring dipoles causes a variation in precessing frequency which results in phase dispersion. Inhomogeneities in the static field also produce a distribution of precessional frequencies across the sample. Primarily as a result of field inhomogeneity, the free precessional signal is destroyed in a short time as the tiny magnets fan out in the perpendicular (x-z) plane, some precessing faster, others slower than average (Figure 2c).

At a time $\tau < T_1$ or T_2, a second rf pulse of sufficient duration to rotate each moment 180° with respect to the x-axis is applied. Because of this reflection about x, those nuclei which had attained a phase lead are now lagging and the slower ones are leading (Figure 2d). When the rf pulse is stopped, precession again continues around the field $\overline{H}_0$. The phase coherence lost because of field inhomogeneities is now regained at the same rate at which it was lost (Figure 2e).

As phase coherence is re-established, a signal is again generated in the pickup coil with the maximum amplitude occurring at time 2τ (Figure 2f), after which phase coherence is lost again. The peak amplitude of this "spin-echo" is less than that of the 90° free precession signal because of spin-lattice and spin-spin relaxation. Figure 3 shows a simulation of the oscilloscope trace of the 90°-

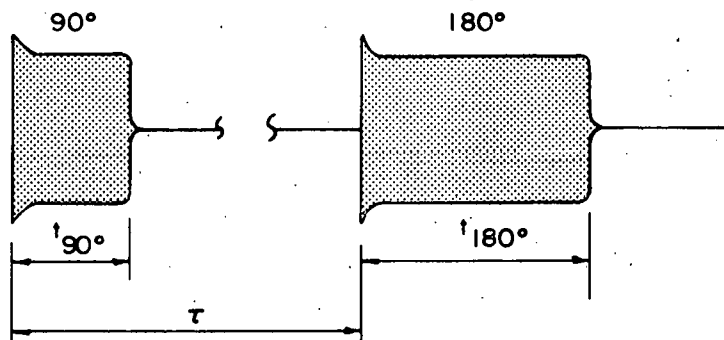Figure 3a. 90° and 180° pulse shapes as viewed on the oscilloscope
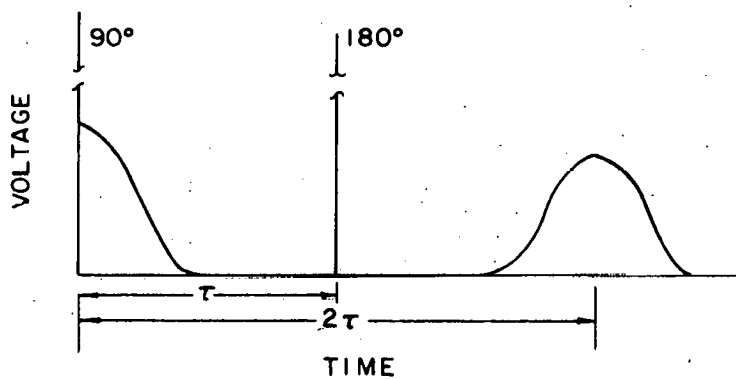
Figure 3b. Simulation of oscilloscope trace of the 90° precession signal and the spin-echo

180° pulse sequence and the precession signals of these pulses followed by the spin-echo.

Mathematical Analysis of Spin-Echo NMR

The natural phenomenon of spin-echo NMR represents a very unique research tool because the entire procedure can be described mathematically with a minimum number of assumptions. Because of the precision with which mathematics describe this technique, a quite complete derivation is provided.

Hahn (18) derived an expression for the effect of molecular diffusion on the spin-echo from a 90°-90° pulse sequence using a phase probability function to account for particle movement. Carr and Purcell (9) approximated molecular diffusion by a random walk technique and obtained a similar expression for the attenuation of the spin-echo of a 90°-180° pulse sequence. Experimental results were in close agreement with the theoretical relationships. The relationship was worked out by Torrey (44) using classical mathematics and was again varified by Douglass and McCall (12) who used a probability density function to describe the phase distribution.

Nuclear magnetic resonance measurements have been obtained by the observation of nuclear induction signals when the ensemble of nuclear spins is perturbed periodically by a small radiofrequency magnetic field. A large D.C.

magnetic field $\overline{H}_0$ establishes an oriented net spin distribution between the high and low energy levels at thermal equilibrium. This produces a resultant magnetic moment $\overline{M}_0$ aligned parallel to $\overline{H}_0$. The forced motion, nutation, of $\overline{M}_0$ results from subjecting the spin ensemble to a rotating rf field $\overline{H}_1$ normal to $\overline{H}_0$. For resonance, the rf field must be of frequency $\omega = \omega_0$, where $\overline{\omega}_0 = \gamma \overline{H}_0$. The magnitude of the static field $\overline{H}_0$ is equal the angular displacement divided by the gyromagnetic ratio

$$|H_0| = \frac{2\pi\omega_0}{\gamma} \tag{25}$$

The net moment is the summation of individual moments $\overline{M}_0(\omega)$, where ω varies due to inhomogeneities in the magnetic field.

The precession of $\overline{M}$ can be described by the torque equation

$$\frac{d\overline{M}}{dt} = \gamma (\overline{M} \times \overline{H}) \tag{26}$$

if damping relaxation affects are neglected.

The description of induction affects can be best explained by transforming to a coordinate system in which the x-z plane is rotating at angular frequency ω_0. If one considers a moment precessing in this rotating system, the torque on the moment due strictly to the rotation is given by $L = \overline{M} \times \overline{\omega}_0$, where $\overline{\omega}_0 = (0, \omega_0, 0)$. Then to a

stationary observer outside the system, the total torque is,

$$\frac{d\overline{M}}{dt} = \frac{D\overline{M}}{dt} + \overline{M} \times \overline{w}_O \tag{27}$$

where $\frac{D\overline{M}}{dt}$ is the torque observed in the rotating system and $\overline{M} \times w_O$ is the torque resulting from system rotation w_O. Considering only the torque observed in the rotating system

$$\frac{D\overline{M}}{dt} = \gamma \, (\overline{M} \times \overline{H}) \; - \; \overline{M} \times \overline{w}_O \tag{28}$$

or by vector mathematics,

$$\frac{D\overline{M}}{dt} = \overline{M} \times (\gamma \, \overline{H} - \overline{w}_O) \tag{29}$$

Because the individual moments rotate in distinctive local fields $\overline{H}_O = \frac{\overline{w}}{\gamma}$ where $\overline{H}_O = (0, H_O, 0)$, and

$$\frac{D\overline{M}}{dt} = \overline{M} \times (\overline{w} - \overline{w}_O) \tag{30}$$

If the mean moment vector rotates at w_O then the precession torque on this vector as observed in the rotating system will be

$$\frac{D\overline{M}}{dt} = \overline{M} \times (\overline{w}_O - \overline{w}_O) = 0 \tag{31}$$

and the moment will appear stationary. All other moments will appear to precess slowly with respect to the rotating system, some faster, some slower.

If the applied magnetic field inhomogeneity is assumed linear then

$$\bar{H}_0(t) = \bar{H}_0 + Gy(t) \qquad (32)$$

where $\bar{H}_0$ is the static field parallel to the y-axis, G is the uniform magnetic field gradient in the y direction and y(t) is the instantaneous position in the y direction measured from the center of the tube.

With this linear field gradient which is provided by the experiment, and by assuming no gradient in the x and z directions, the representation of the moments in a rotating system before the rf pulse would be as follows. All moments in the (x, 0, z) plane will appear stationary. Moments in (x, y > 0, z) planes will precess progressively faster, and moments in (x, y < 0, z) planes will precess progressively slower. A representation of the $\bar{M}(y)$ net moments is shown in Figure 4a.

Consider these moments when a rf pulse at frequency w_0 is applied. This produces a magnetic field $\bar{H}_1$ of frequency w_0 which rotates in the x-z plane. This oscillating field can be represented as two vectors:

$$\bar{H}_{1_L} = (\frac{H_1}{2} \cos w_0 t, \ 0, \ \frac{H_1}{2} \sin w_0 t) \qquad (33)$$

$$\bar{H}_{1_R} = (\frac{H_1}{2} \cos (-w_0)t, \ 0, \ \frac{H_1}{2} \sin (-w_0)t)$$
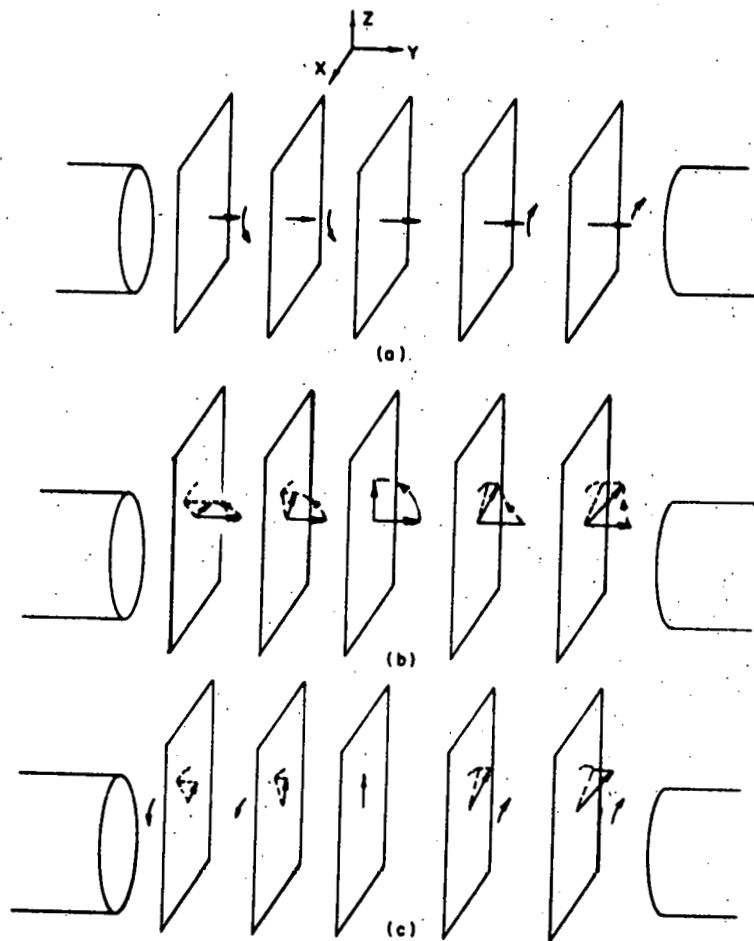
Figure 4.   Influence of static field gradient on
            precession and nutation (exaggerated dif-
            ferential motion)

which rotate in opposite directions. Since it has been established that to have an effect the field must rotate at $(+ \omega_o)$, the $\overline{H}_{1_R}$ field, which rotates at $- \omega_o$, may be neglected. The nutation torque on each net moment $\overline{M}(y)$ is

$$\frac{D\overline{M}(y)}{dt} = \overline{M} \times (\overline{\omega} - \overline{\omega}_o + \gamma \overline{H}_1) \qquad (34)$$

From this, only the $\overline{M}(0)$ moment will be nutated directly into the x-z plane. The other moments $\overline{M}(y)$ will precess either positive or negative with respect to ω_o during nutation, and the resultant ensemble on removal of the $90°$ pulse, will be as shown in Figure 4b. The magnitude of the rf pulse is determined by the relationship of Equation 25. Precession is now in the y-z plane, and ω is equal to the reciprocal of four times the duration of the $90°$ pulse.

$$|H_1| = \frac{2\pi(\frac{1}{4 \ t_{90}})}{\gamma} \qquad (35)$$

After the $90°$ pulse, the torque is again given by Equation 30, however, now $\overline{M}(y)$ is in the x-z plane and the torque causes rotation in that plane, some forward, some backward, with $\overline{M}(0)$ stationary in the rotating system as shown in Figure 4c. Moment rotation in the x-z plane cuts lines of force of the applied field $\overline{H}_0$ and induces a voltage.

Effects of natural relaxation

The signal generated by these rotating moments begins to decay immediately. Natural inhomogeneities and relaxation effects provide damping of the torque equations. Effects such as internal fields due to neighboring nuclei and the forces due to thermal lattice vibration must be included. Although these fields are much weaker than externally applied fields, they are of importance because their cumulative affects act over a longer period of time.

Consider a finite moment $\overline{M}$. The effects on it due to thermal agitation and internuclear action can be explained in the following manner. The two actions are similar but with one essential difference, only thermal agitation can change the energy of the total spin system. Internuclear actions leave the total energy constant. The dominant part of the total spin energy E_n is caused by the strong external field $\overline{H}_0$ in the y direction.

$$E_n = -H_0 M_y \tag{36}$$

Major changes in the total energy are therefore necessary due to a change of the polarization and it will be the thermal agitation which will be responsible for these changes. The equilibrium value that M_y will approach under the influence of thermal agitation is given by

$$\overline{M}_0 = x \overline{H}_0 \tag{37}$$

where X is the magnetic susceptibility.

If at any time $M_y \neq M_0$, it will approach this value exponentially with the characteristic time constant T_1, the thermal or longitudinal relaxation time. We can describe the rate of change of M_y, due to thermal agitation alone by

$$\frac{dM_y}{dt} = - \frac{(M_y - M_0)}{T_1} \tag{38}$$

which gives

$$\frac{M_y}{M_0} = 1 - e^{-\frac{t}{T_1}} \tag{39}$$

This describes the rate at which a vector in the x-z plane tends to return to the $\overline{H}_0$ orientation. It is also the time for randomly oriented moments to align when placed in a strong magnetic field.

For most substances, T_1 is quite long, but by the addition of a small amount of paramagnetic material the time can be shortened greatly. The molecules of the paramagnetic substance act essentially as catalysts, with the relatively strong fields of their permanent magnets greatly reducing the relaxation time T_1.

Fields due to neighboring nuclei also contribute to the establishment of the equilibrium because of their thermal agitation. These fields are so small that alone

they would lead to extraordinarily long thermal relaxation times with the influence being negligible. Internuclear actions can, though, be of importance for the changes of the other two components, M_x and M_z. The fact that the nuclei of their moments participate in the thermal agitation is of minor importance to M_x and M_z because they are only effected by changes which do not change the energy of the total spin system. These changes, in M_x and M_z can, therefore, take place without the necessity of transferring spin energy E_n into kinetic energy of the atoms.

Processes in which the total spin energy does not change and which therefore affect only the M_x and M_z components are not necessarily due to internuclear forces alone. Small, irregular inhomogeneities in $\bar{H}_0$ and the presence of other moments such as paramagnetic ions will cause similar affects. Such action on M_x and M_z can be described including internuclear effects, by an effective irregularity of the y field of order $\bar{H}'$. Then with this field one has a "transversal" relaxation time, T_2, which is the time necessary for M_x and M_z to be appreciably affected. T_2 is a time constant characterizing the rate at which M_x or M_z decrease.

$$T_2 = \frac{1}{\gamma |H'|} \tag{40}$$

The effect of the "transversal" relaxation time is considered to be exponential. Thus,

$$\frac{dM_x}{dt} = -\frac{M_x}{T_2} \quad ; \quad \frac{dM_z}{dt} = -\frac{M_z}{T_2} \tag{41}$$

and

$$\frac{M_x}{M_{xo}} = e^{-\frac{t}{T_2}} \tag{42}$$

The same equation is used for M_x and M_z because the system is assumed to be isotropic.

The total rate of change of $\overline{M}$ is obtained by adding the three effects 1) external forces, 2) longitudinal relaxation, and 3) transverse relaxation. The three components of $\overline{M}$ are then

$$\frac{dM_x}{dt} - \gamma (M_y H_z - M_z H_y) + \frac{M_x}{T_2} = 0$$

$$\frac{dM_y}{dt} - \gamma (M_z H_x - M_x H_z) + \frac{(M_y - M_o)}{T_1} = 0 \tag{43}$$

$$\frac{dM_z}{dt} - \gamma (M_x H_y - M_y H_x) + \frac{M_z}{T_2} = 0$$

or

$$\frac{d\overline{M}}{dt} = \gamma (M \times \overline{H}) - \frac{1}{T_2} (M_x + M_z) - \frac{1}{T_1} (M_y - M_o) \tag{44}$$

This torque equation is not written in the rotating
coordinate system.

Effect of diffusion

The effect of particle motion produces a signal
attenuation in addition to those discussed in the preced-
ing development. Particle diffusion increases the rate of
phase dispersion because the average field seen by a
particular nucleus between times 0 and τ is not necessarily
the same field seen by this nucleus between times τ and 2τ.
When a particle moves into a different magnetic field its
precession rate changes. As a result, the phase lost
between 0 and τ will not in general be the same as the
phase coherence regained by time 2τ.

To measure the effect of diffusion it is necessary to
create a field gradient in the y direction. The gradient
G is obtained by placing symmetrically on each side of
the sample a circular coil of wire. The current directions
should be such that the fields oppose each other. The
gradient must be small though so $H_1 \gg \sigma$, where σ is the
standard deviation of the y field. This is required so
that the individual nuclear moment frequencies will be
nearly equal to ω_o, and thus will all be nutated very near
to the x-z plane by the 90° pulse (Figure 4). In addi-
tion, if the value of G is calculated from the current in
the wires it is necessary that G be large compared to the

average gradient in the field due to the magnet. Figure 5
shows the opposing coils and how they produce a linear
gradient in the y direction. The theory and design informa-
tion for the gradient coils is given in Tanner (39).

The effect of diffusion can be analyzed by considering
the motion in the y direction to be represented by random
discrete steps. For simplicity we assume that a molecule
remains in a given y position exactly t' seconds, then
abruptly jumps to a new position whose y coordinate differs
from the previous one by ba_i, where b is a fixed distance
and a_i, a random variable whose value is either 1 or (-1).

The gradient of $\overline{H}_0$ in the y direction is constant and
of magnitude G, gauss/cm. Let $H_y(0)$ be the field in which
a given nucleus is located at t = 0. At some later time
t = jt' the nucleus will be in a field $H_y(jt')$ given by

$$H_y(jt') = H_y(0) + Gb \sum_{i=1}^{j} a_i \tag{45}$$

After N steps, at t = Nt', the phase angle ϕ of the pre-
cessing moment of this nucleus will differ from the value
ϕ_0 it would have had at this same time if the nucleus had
remained in the initial y location. The change in pre-
cession angle is given by

$$\phi_D = \phi - \phi_0 = \sum_{j=1}^{N} \gamma t' [H_y(jt') - H_y(0)] \tag{46}$$

$$\overline{H} + GY$$

$$\overline{H}_o$$

$$H_R$$ $$H_L$$

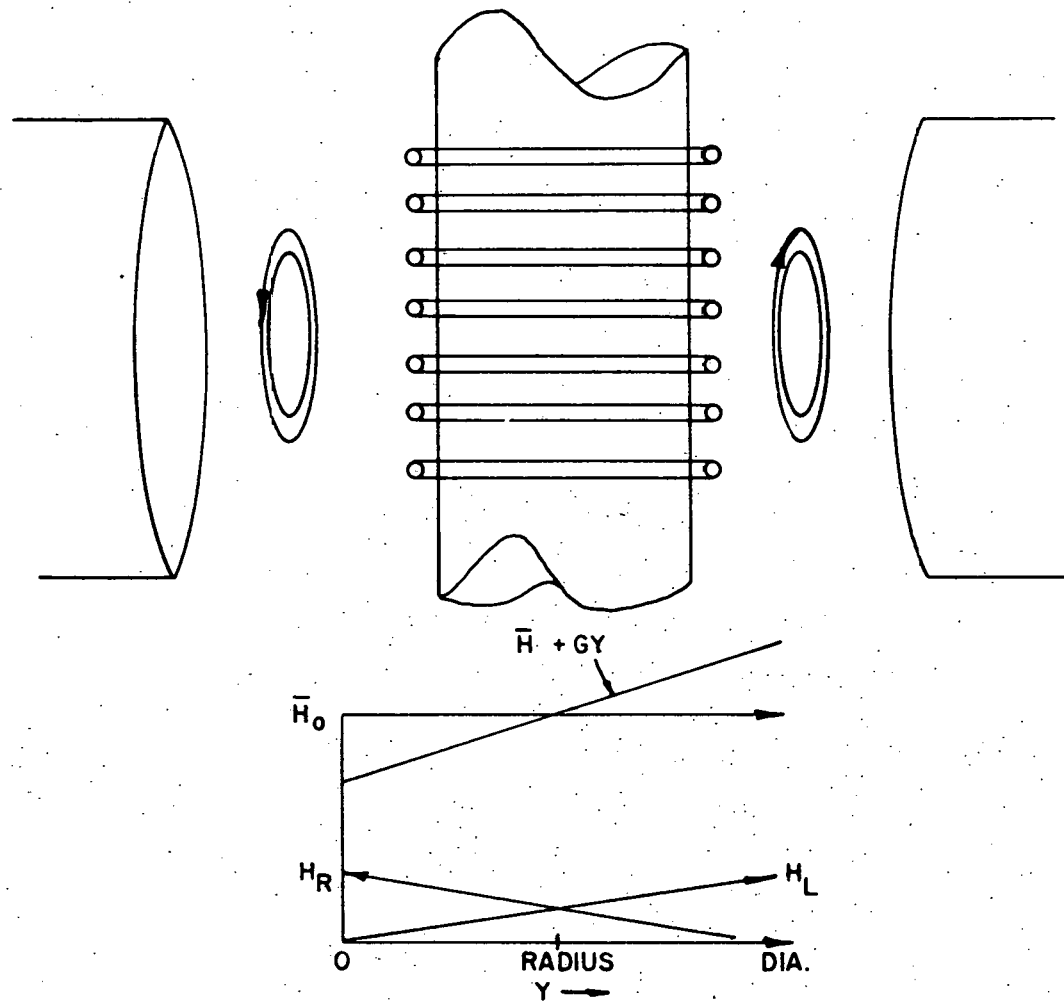O   RADIUS   DIA.

$$Y \longrightarrow$$

Figure 5. Gradient of the static magnetic field

Of major interest here is the change in the rate of pre-cession and the resulting discrepancy in phase caused by the transport of the nucleus into a region where the applied field is different. Substituting for $H_y(t)$

$$\phi_D = Gb \gamma t' \sum_{j=1}^{N} \sum_{i=1}^{j} a_i = Gb \gamma t' \sum_{j=1}^{N} (N + 1 - j) a_i \tag{47}$$

Since the a_i's are random

$$\phi_D = Gb \gamma t' \sum_{j=1}^{N} ja_i \tag{48}$$

This distribution will be Gaussian in the limit of large N. So

$$< \phi_D^2 >_{avg} = G^2 b^2 \gamma^2 t'^2 \sum_{j=1}^{N} j^2$$

$$= G^2 b^2 \gamma^2 t'^2 N(N + 1)(\frac{2N + 1}{6}) \tag{49}$$

If N is large the lower powers of N can be dropped and one can also transfer from random steps to continuous diffusion. By comparing the solution to the diffusion equation

$$D\nabla^2 f = \frac{df}{dt} \tag{50}$$

where $f(x, y, z)$ is the probability density, then

$$D = \frac{b^2}{2t'} \tag{51}$$

and

$$< \phi_D^2 >_{avg} = \frac{2 \; G^2 \; \gamma^2 \; Dt^3}{3} = \sigma^2 \tag{52}$$

where σ is the standard deviation of $\bar{H}_0(y)$. The distribution in phase of the moments across y after time t will be

$$P(\phi_D) = (\frac{4\pi \; \gamma^2 \; G^2 \; Dt^3}{3})^{-1/2} \; e^{- \frac{3 \; \phi_D^2}{4G^2 \; \gamma^2 \; Dt^3}}$$

$$= \frac{1}{\sqrt{2\pi \; \sigma^2}} \; e^{- \frac{\phi_D^2}{2 \; \sigma^2}} \tag{53}$$

which represents the normal or Gaussian distribution. The intensity of the generated echo at time t is then a summation over the frequency range

$$|\bar{M}|(t) = |\bar{M}_0| \int_{-\infty}^{\infty} \cos \phi_D \; P(\phi_D) \; d\phi_D \tag{54}$$

for the echo following the 90° pulse.

$\bar{M}(t)$ may be thought of as $M_x(t)$ in the rotating system. The moment magnitude varies as expressed by Equation 54, and it rotates at ω_0 generating the voltage represented by the 90° precession signal as shown on Figure 3. Since the probability distribution of the phase dispersion across the sample in the y direction is Gaussian, Equation 54 integrates to

$$|\bar{M}|(t) = |\bar{M}_0| \; e^{- \frac{\gamma^2 G^2 \; Dt^3}{3}} = e^{- \frac{\sigma^2}{2}} \tag{55}$$

However, the echo after the 180° pulse is of prime importance. The effect on Equation 47 will be to reverse the signs of all terms beyond $j = \frac{\tau}{t'}$. If during the time interval $t = Nt'$, one 180° pulse was applied at $t = \frac{Nt'}{2}$, then

$$\phi_D = \phi - \phi_0 = Gb\,\gamma t' \sum_{j=1}^{N} c_j \sum_{i=1}^{j} a_i \tag{56}$$

where $c_j = 1$ from $0 < j < \frac{N}{2}$, $= -1$ from $\frac{N}{2} < j < N$. This gives

$$<\phi_D^2>_{avg} = G^2 b^2 t'^2 \gamma^2 \left[\frac{N^3}{12} - \frac{N}{6}\right] \tag{57}$$

and in the limit of large N

$$<\phi_D^2>_{avg} = \frac{G^2 \gamma^2 D t^3}{6} = \sigma^2 \tag{58}$$

The intensity of the echo at any time t is given by

$$|\overline{M}|(t) = |\overline{M}_0| \int_{-\infty}^{\infty} \cos\phi_D\, P(\phi_D)\, d\phi_D = |\overline{M}_0|\, e^{-\frac{\gamma^2 G^2 D t^3}{12}} \tag{59}$$

Thus, decay caused by diffusion plus natural relaxation produces echo attenuation with time expressed as

$$|\overline{M}|(t) = |\overline{M}_0|\, e^{-\frac{t}{T_2} + \left(-\frac{\gamma^2 G^2 D t^3}{12}\right)} \tag{60}$$

For the diffusion effect to be significant,

$$\frac{12}{\gamma^2 G^2 D} \leq T_2^3 \tag{61}$$

or the transverse relaxation will dominate the attenuation.

Gradient calibration

The preceding derivation of the shape of the spin-echo contains no reference to the volume of the sample. The diffusion coefficient D refers to the average volumetric value, and the shape of the sample is actually accounted for by the gradient term G.

Taking logarithms, Equation 60 is

$$\ln \frac{|\overline{M}|(t)}{|\overline{M}_0|} = -\frac{t}{T_2} - \frac{\gamma^2 G^2 D t^3}{12} \tag{62}$$

If $\ln \frac{|\overline{M}|(t)}{|\overline{M}_0|} + \frac{t}{T_2}$ is plotted against t^3 the value of D can be calculated from the slope of the straight line curve. These data must be obtained with a constant field gradient and diffusion time. Error in determining the slope will introduce uncertainty to the value of D.

The curve is also influenced by the value of T_2. The correct value for T_2 is quite difficult to measure. An alternative method may be used to determine diffusion coefficients, and it provides the basis for measurement of particle motion in a dynamic system. The system requirement of Equation 60 is a constant volume sample. When a flowing sample is measured over a range of times, sample

volume will change and the constant D cannot be determined. However, if the data is obtained at fixed diffusion time, ln $M(t)$ can be plotted against G^2 and the diffusion coefficient D calculated from the slope. For a turbulent sample the particle movement is much greater, and the constant D is actually $E(t)$, the turbulent diffusivity. Although the data are obtained for a flowing sample, the system volume remains constant because the flow rate and diffusion time are not varied.

This technique makes it unnecessary to measure T_2, but a precise measurement of the magnetic gradient is mandatory since the values of G are squared. Because the gradient is provided as in Figure 5, an accurate measure of the current through the coils can be used to determine G.

As stated, the value of G in Equation 60 incorporates the sample shape. The sample shape determines the relationship between the gradient and the current through the gradient coils.

For a symmetrical gradient imposed on the field $\overline{H}_0(y)$ the signal, at any time t, of the 90° pulse is given by

$$|\overline{M}|(t) = |\overline{M}_0| \int_{-\infty}^{\infty} f(\overline{H}_0(y)) \cos \gamma (\overline{H}_0(y) - \overline{H}_0(0))t \, d\overline{H}_0(y)$$

(63)

which is summed across the frequency range at a given time. For a linear gradient, $f(\overline{H}_0(y))$ is represented by an equal

distribution of field from $\overline{H}_0(-r)$ to $\overline{H}_0(r)$ as shown in Figure 6a. The magnitude of the average moment is

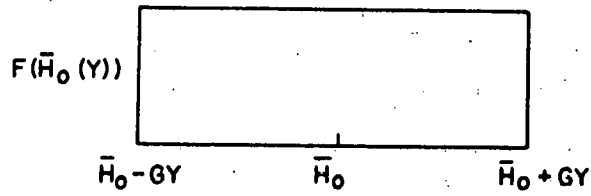$$|\overline{M}|(\omega) = \frac{|\overline{M}_0|}{\text{CSA of sample} * \text{Gradient}} \tag{64}$$

Then $\overline{M}(\omega)$ is multiplied by the sample width for which it applies. As a simple example, assume a square sample as shown in Figure 6b. Then

$$|\overline{M}|(t) = \int_{-\infty}^{\infty} \frac{|\overline{M}_0|}{4Gy^2} (2y) \cos \gamma (\overline{H}_0(y) - \overline{H}_0(0)) t d\overline{H}_0(y)$$

$$= \frac{|M_0|}{2Gy} \int_{H_0(0) - Gr}^{H_0(0) + Gr} \cos \gamma (\overline{H}_0(y) - \overline{H}_0(0)) t d\overline{H}_0(y)$$

$$= |\overline{M}_0| \frac{\sin \gamma Gyt}{Gy \gamma t} \tag{65}$$

This relationship of the 90° echo shape with G could then be used to calibrate the gradient coils.

A more useful calibration would be for a cylindrical sample (Figure 6c). Then

$$|\overline{M}|(t) = \int_{-\infty}^{\infty} \frac{|\overline{M}_0|}{G\pi r^2} (2r \sin \theta) \cos \gamma (\overline{H}_0(y) - \overline{H}_0(0)) t d\overline{H}_0(y)$$

$$= \int_{\overline{H}_0(0) - Gr}^{H_0(0) + Gr} \frac{2|M_0|\sin \theta}{G\pi r} \cos \gamma (Gy) t (Gdy)$$

$F(\bar{H}_o(Y))$

$\bar{H}_o - GY$　　　$\bar{H}_o$　　　$\bar{H}_o + GY$

(a)

2 r

$\dfrac{|\bar{M}_o|}{4GY}2$

$\bar{H}_o - GY$　　　$\bar{H}_o$　　　$\bar{H}_o + GY$

(b)

$\dfrac{|\bar{M}_o|}{\pi Gr^2}$

r

θ

$\bar{H}_o \cdot Gr$　　　　　　$\bar{H}_o + Gr$

$\bar{H}_o$
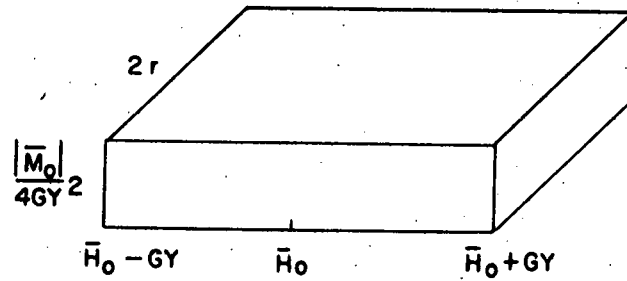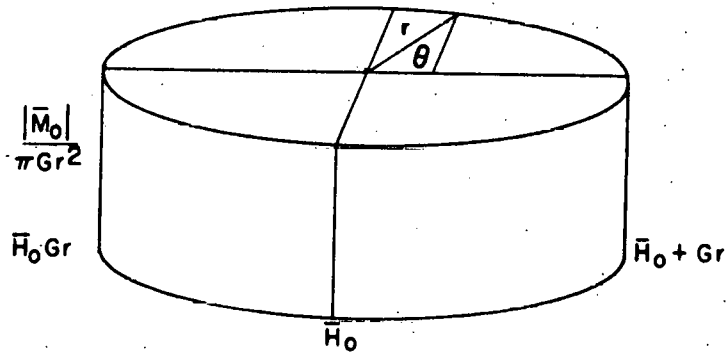
(c)

Figure 6.　Moment distribution for different sample shapes

$$= \int_{\pi}^{0} \frac{2|\overline{M}_0|}{G\pi r} \sin\theta \ (\cos\gamma(Gr\cos\theta)tG(-r\sin\theta d\theta)$$

$$= \frac{2|\overline{M}_0|}{\pi} \int_{0}^{\pi} \sin^2\theta \cos(\gamma \, Gr \, t \cos\theta)d\theta$$

$$= \frac{2|\overline{M}_0| \, J_1 \, (\gamma \, Grt)}{\gamma \, Grt} \tag{66}$$

Equation 66 provides the relationship required to calibrate the gradient for a cylindrical sample. Measurement of the time required for the $90°$ precession signal to decay at different current settings determines G as a function of gradient coil current.

Effect of Flow

Although the technique of obtaining diffusivity data at fixed times by varying gradient permits measurements to be made with dynamic samples, there is a flow characteristic which must be considered. In spin-echo NMR measurement only moments which remain in the sample for the entire diffusion time contribute to the spin-echo peak voltage. In a turbulent flowing sample a velocity profile is established, and more moments in the fluid nearer the pipe wall contribute to the signal at time 2τ since the particles in the center of the tube have left the receiving coil. Therefore, at longer observation times and higher rates the sample con-

tains progressively larger percentages of the moments near the wall, and the diffusivity value is no longer an average volumetric quantity. In the extreme, this explains why the spin-echo technique is limited to a small range of flow rates and diffusion times, since moments must remain within the volume of the receiving coil for the time 2τ to induce the spin-echo signal.

Calculation of Diffusion Parameters in a Flowing Sample

The peak amplitude of the spin-echo may be expressed as

$$|\overline{M}|(t) = |\overline{M}_0|A(t) e^{-\frac{\gamma^2 G^2 kt^3}{12}} \qquad (67)$$

where $A(t)$ describes the attenuation of the spin-echo by effects other than diffusion. The factor k accounts for diffusion effects and equals either the molecular diffusion coefficient or the diffusivity depending upon flow rate.

As discussed with respect to gradient calibration, the traditional technique for obtaining k experimentally is to plot $\ln \frac{|\overline{M}|(t)}{A(t)}$ versus t^3 and calculate k from the slope (9, 12). $A(t)$ can be determined by measuring spin-echo attenuation with zero gradient. Woessner (45) proposed another method by which $|\overline{M}|(t)$ is measured at a function of G at a fixed value of t. The slope of a plot of $\ln |\overline{M}|$ versus G^2 is used to calculate k. This procedure offers more simplicity in operation since the pulse sequence timing

need not be varied during a run, and it is not necessary to measure $A(t)$. This gradient plot procedure also allows examination of a flowing sample, which would not be possible by the time variant technique.

EXPERIMENTAL WORK

NMR Equipment

The spin-echo NMR equipment consisted of a pulse genera-
tion system, electromagnet with power supply, sample coil,
amplifying equipment and a means of displaying the induced
voltage signal. A diagram of the spin-echo NMR circuit is
shown in Figure 7. The following is specifications on the
equipment.

1. Electromagnet--Varian Associated Model V-3700-1
   water cooled magnet, 6-inch dia. cylindrical pole
   caps, 1-1/4-inch air gap, field deviation not to
   exceed 0.1 gauss within 2.7 cm of pole cap axis.

2. Magnet power supply--Varian Associated Model V-2900,
   2 KW, current regulation to within 10 ppm for $\pm$ 10
   percent line or load changes, field ripple less
   than 10 milligauss peak-to-peak in air gap.

3. Trigger pulse generator--Magnion, Inc. Model PG-
   302 pulse programmer, individual pulse width
   control from 1 to 10 microseconds, delay time
   range 100 microseconds to 2 seconds, sequence
   recycle periods from 10 msec to 20 sec with both
   automatic and manual options.

4. 10 MC/sec exciter--Magnion, Inc. Model TF-311,
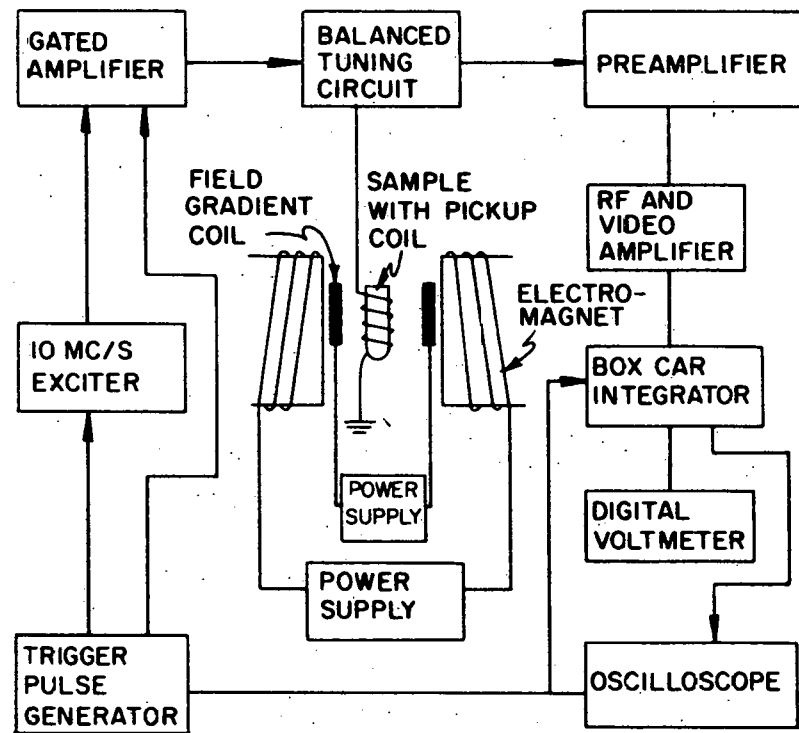   10 watt power output.

Figure 7.   Schematic diagram of the spin-echo NMR circuit

5. Gated amplifier--Arenburg Ultrasonics pulsed
   oscillator Model PG-650-C, converted to gated
   amplifier operation, 100 watts peak power output.

6. Balanced tuning circuit--Twin coil balanced net-
   work.

7. Preamplifier--Arenberg Ultrasonics Model PA-620-B,
   gain 35 db.

8. Amplifier--Arenberg Ultrasonics Model WA-600-C
   wide band amplifier, gain 85 db, 10 volt maximum
   detector stage output, recovery from extreme over-
   load in less than 0.1 msec.

9. Oscilloscope--Tektronic, Inc. type 561 with a type
   3A1 DC to 15 MC/sec amplifier and a type 3B3 time
   base with delayed sweep triggering.

10. Boxcar integrator--Princeton Applied Research
    Model CW-1, 10 volt maximum output with input
    sensitivity adjustment from 0.2 to 100 volts, time
    base range from 10 microseconds to 1 second, gate
    width adjustable from 10 to 100 percent of time
    base, and time constant range 0.1 msec to 100 sec.

11. Digital voltmeter--Hewlett Packard Model 3440A
    with a 3443A high gain-auto range plug-in unit,
    five digit read-out with voltage ranges of 10,
    100, and 1000 volts and accuracy of better than
    0.05 percent of reading.

Circuit components 3 through 9 were operated from a Sorenson Model ARC 1000 AC regulator providing supply voltage regulation to 0.1 percent.

The sample coil, which was both the rf pulse transmitter and the response signal receiver, consisted of 11 turns of number 20 Nyclad copper wire 3/8 inch in length with an inside diameter of 0.475 inches. The gradient coils had 12 turns each of number 20 Nyclad copper wire with a mean radius of 0.625 inches and a separation distance of 0.52 inches. The arrangement of the pickup coil-gradient coils, as illustrated in Figure 8, was mounted in a split plexiglass block. Direct current was supplied to the gradient coils by a Lambda Model LH 127 FM current regulated power supply, which was modified by an integrated circuit to give current regulation to $\pm$ 0.01 percent. The plexiglass block was held rigidly in the magnetic field by a brass support arm bolted to the magnet frame.

The set of rf pulses were generated in the gated exciter as low power 10 MC/sec rf signals. These signals were then amplified and squared off (fast rise time) in the gated amplifier. The trigger pulse generator determined the length of each pulse, and also the time between pulses. The 10 MC/sec rf output was connected to the sample coil through a tuning network and the resonance frequency of the tuning circuit was matched with the frequency of the rf out-

POLE CAP AXIS

SAMPLE TUBE

PICKUP
COIL

CURRENT
FLOW

$\bar{H}_{I_L}$

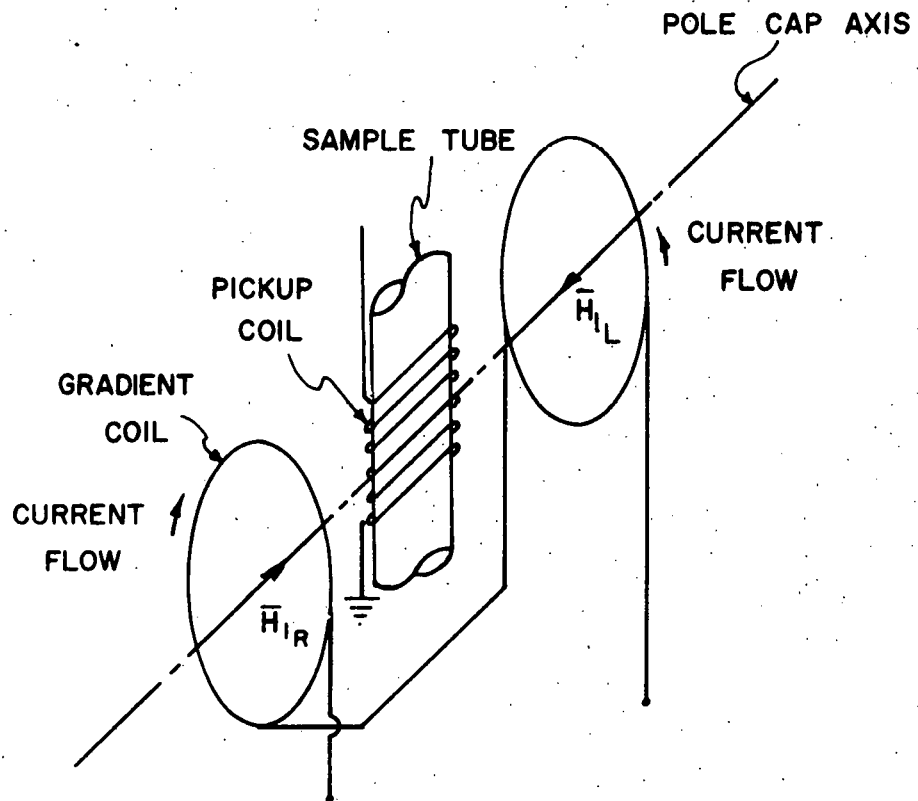GRADIENT
COIL

CURRENT
FLOW

$\bar{H}_{I_R}$

Figure 8. Sample and field gradient coil arrangement

put. Then by varying the magnetic field strength the Larmor frequency of the hydrogen nuclei was changed to a mean frequency of 10 MC/sec.

Flow System

The gravity flow system used for this study is shown schematically in Figure 9. A steady flow of water at room temperature was obtained from a constant head tank; the flow rate was measured with a calibrated rotometer. The flow tube was supported in a vertical position by a rigid aluminum framework which was fitted with clamps for alignment.

Water was recirculated in the system by a Randolf roller pump which was chosen over a centrifugal pump because it added only a negligible amount of heat to the water. The room temperature in the area of the equipment was thermostatically controlled to 25° C. The water temperature changed less than 0.3° C during an experimental run even though water temperature was not regulated by heat exchange.

A glass tube, 0.405 cm dia. with a standard dia. deviation of less than 0.002 cm, was used in this research. There was a length 248 tube diameters of straight tube for flow profile development preceding the sample coil.
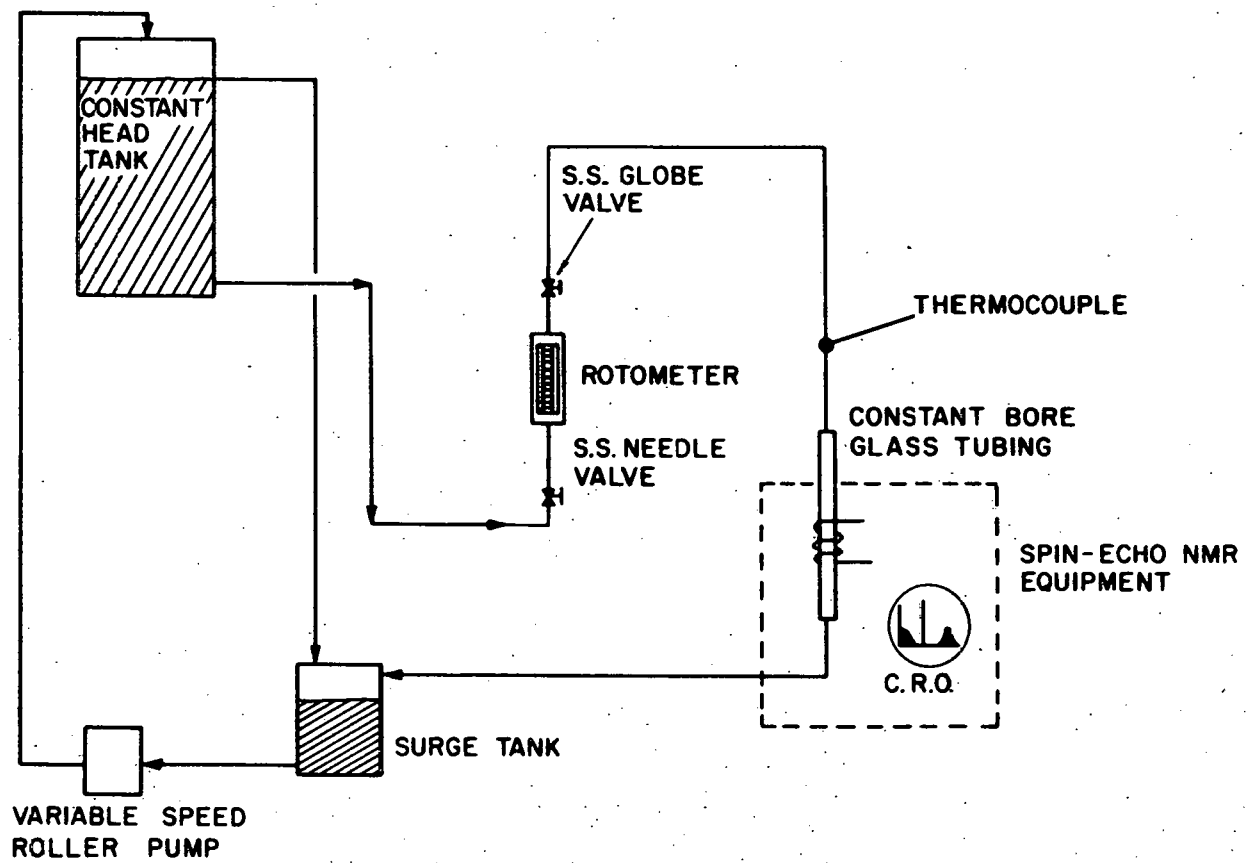
Figure 9. Schematic diagram of the flow system

Experimental Procedure

The spin-lattice relaxation time, T_1, of distilled water is quite long, approximately one second. Since this is a measure of the time required for moment orientation in a magnetic field, it is necessary to reduce this time when studying flowing systems. Time constants T_1 and T_2 were artificially shortened by the addition of a small amount of paramagnetic salt ($MnCl_2 - 2H_2O$). This was not a critical concentration, a solution of 0.0005 to 0.001 M $MnCl_2 - 2 H_2O$ was satisfactory. The catalytic action of the paramagnetic ions is quite complex. A detailed discussion of the relaxation processes and the artificially shortening interaction is given by Pake (28).

The procedure for tuning spin-echo NMR circuits and the establishment of the 90°-180° pulse sequence has been described in detail by Schwartz (34). After the circuit was tuned, each pulse width was set. To determine the length of the 90° pulse, the programmer was set at the time corresponding to the first maximum of the 90° induction signal (Figure 3).

Because it is much easier to determine the minimum or zero induction signal than a maximum value, the preferred procedure is to first set the time duration of the 180° pulse. This represents nutation from the y to (-y) direction on Figure 2. The 90° pulse is then set for

exactly one-half the power of the 180° pulse.

The correct 180° pulse was placed on the scope and a photograph of it taken. The area of the pulse was then measured with a planimeter. Since the area is proportional to the pulse power, the 90° pulse could then be set very accurately. The 90°-180° sequence consisted of pulses of 2.5 and 5.0 microseconds in length with a voltage of 800 volts peak-to-peak. During the course of the research some of the pulse generation equipment had to be repaired. Peak-to peak voltage had dropped to 325 volts, with pulse times of 11.5 and 23.0 microseconds. This variation in pulse length did not appear to affect the data. The magnitude of the generated rf magnetic field, $|\bar{H}_1|$, as given by Equation 35, for the 800 volt pulses was 23.5 gauss.

Calibration of the oscilloscope time base was checked. The values of 2τ in each run were set by using the boxcar integrator gate as a mark, then by using the delayed sweep of the scope the time between pulses could be adjusted very accurately. The accuracy in positioning the gate was about $\pm$ 0.01 divisions. The pulse delay time was set exactly, so the time measurement accuracy was a minimum of $\pm$ 0.1 percent.

The echo amplitudes were measured with a boxcar integrator. This instrument is essentially a well con-trolled capacitor which is charged to the average voltage

at that point on the signal that is being measured. By repeated measurements, with the gate of the integrator aligned with the peak of the spin-echo, the voltage can be measured accurately even in a noisy signal. The integrator output, always between 0 and 10 volts, was measured with the digital voltmeter. This signal fluctuated for a turbulent sample, but since the logarithm of the voltage was plotted, accuracy to three significant figures provided satisfactory results.

As has been stressed, the value of this technique using the **gradient plot** method of analysis is dependent on the accuracy of the gradient coil calibration. As derived, the shape of the 90° induction signal for a cylindrical sample in a constant field gradient perpendicular to its axis is

$$\frac{M}{M_0} = \frac{2J_1(\gamma Grt)}{\gamma Grt} \tag{68}$$

The coil system is calibrated with a static sample by measurement of the time of the 90° free induction decay. $J_1(\gamma Grt)$ is equal to zero at $t_0 = 0$, and again at $t_1 =$ decay time. Then

$$J_1(\gamma Grt_0) = 0 \quad ; \quad \gamma Grt_0 = 0$$

$$J_1(\gamma Grt_1) = 0 \quad ; \quad \gamma Grt_1 = 3.832$$

$$\gamma Gr(t_1 - t_0) = 3.832$$

$$G = \frac{3.832}{\gamma Gr(t_1 - t_0)} \tag{69}$$

For each value of gradient coil current, Equation 69 gives the field gradient. Photographs of the echo were taken at each current setting. Then the decay time was measured as accurately as possible. As the gradient increased, the zero at t_1 became much sharper. Time measurement accuracy was about $\pm$ 0.1 scale division. The calibration curve used is shown in Figure 10. Several sets of calibration data were taken over the current range of 0 to 500 ma, and the resulting data were fitted by a linear least squares calculation.

Woessner (45) points out certain precautions which must be taken to maintain accuracy when using the gradient plot method. In Equation 67 the numerical term $A(t)$ has been found to be independent of both the rf nutation angles and deviations from exact resonance. However, the echo can be artificially damped by excessive field gradient, because not all the nuclei are nutated through the same angle by the rf pulses as the gradient changes (Figure 4). For valid data the moments must be nutated through the same angle at each gradient. Woessner checked this experimentally by examining the attenuation at very short times so that the exponential term in Equation 67 was unity. The echo amplitude was measured as a function of $Gd/|\bar{H}_1|$. The

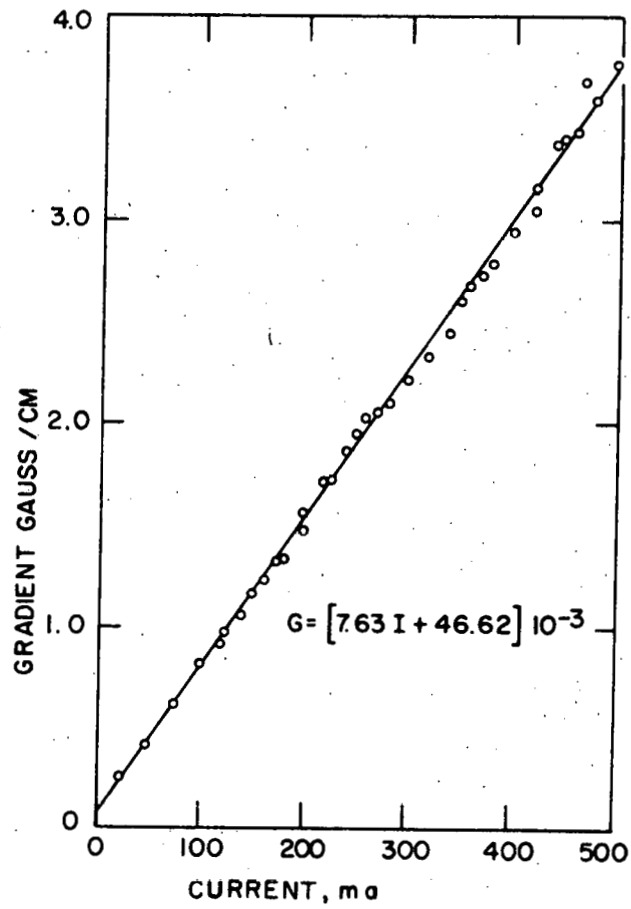$$G = [7.63\, I + 46.62]\, 10^{-3}$$

Figure 10. Calibration curve for the field gradient
            coils

decrease in amplitude was 5 percent when $(Gd/|\bar{H}_1|) = 1$. The percentage damping varied as $5(Gd/|\bar{H}_1|)^2$ up to $(Gd/|\bar{H}_1|) = 3$. For valid data $|\bar{H}_1|$ must be several times larger than Gd. The maximum gradient used in this research was less than 4 gauss so

$$\frac{Gd}{|\bar{H}_1|} = \frac{4(0.81)}{23.5} = 0.1375$$

and the damping error was

$$5(0.1375)^2 = 0.1\%$$

This is a very important limitation to the gradient plot method as compared to the classical method, that of varying time. For samples having either short T_2 values or small diffusion coefficients, or for flowing samples at high rates and short observation time, large magnetic field gradients are necessary to produce echo attenuation.

The diffusivity data were obtained by the following procedure once the pulse times had been set:

1. The time τ between pulses was set. For the minimum calibrated time scale on the oscilloscope greater than τ, a short gating pulse from the boxcar integrator was positioned with the leading edge directly at $t = \tau$. Then the scope was switched to delayed sweep and the gate pulse located again. On this expanded scale the $180°$

pulse was then set at the leading edge of the
gating pulse.

2. The flow rate was set by visual observation of
the rotameter. A motor with gear reduction was
used to accurately set the flow rate.

3. The gradient current was set to a predetermined
value, with the current indication recorded.
Recorder accuracy was 0.1 percent of range, which
was either 125, 250, or 500 ma.

4. The boxcar integrator gating pulse was then
positioned at the peak of the spin-echo. The
sensitivity scale of the integrator was set and
the gain of the video amplifier was adjusted so
that the induced peak voltage at the minimum
gradient value for that run was about 10 volts.
The gate pulse width was then shortened so that
only the peak voltage was integrated, and the
time constant for the integrator was set to give
the optimum fluctuation damping.

5. The voltage value was read from the digital
voltmeter and recorded, then the gradient current
was increased and the peak voltage again recorded.

6. The gradient was usually increased until the
induced peak voltage was about 3 volts.

7. The flow rate was then set at a different value
    and steps 3 to 6 repeated.

The above description represents the technique required
to obtain each individual diffusivity value. The data were
then plotted as explained previously and the diffusivity
value calculated from the slope of the curve. Figure 11
represents this curve for a typical set of data. Four sets
of data were obtained at each of four delay times, and at
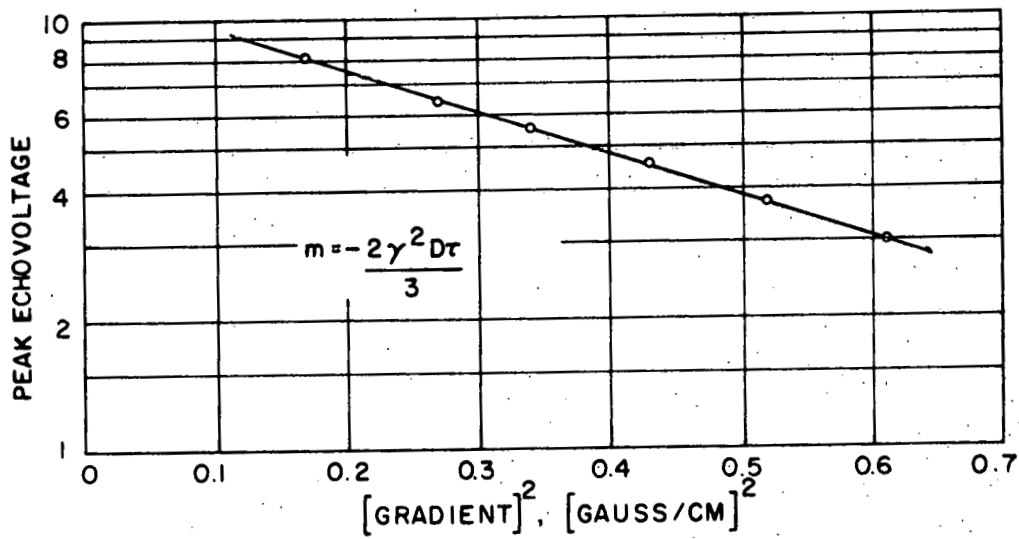seven different flow rates.

Figure 11. Data for determining diffusivity using the gradient plot method

RESULTS AND DISCUSSION

Diffusivity as a Function of Time

Average volumetric unidirectional eddy diffusivity
measurements were made for flowing samples over a range of
rates and diffusion times. Since the assumption of isotropy
is requisite for a statistical study of turbulence, and was
also made in the mathematical NMR derivations, the diffu-
sivities can be termed actual volumetric quantities.

The effect of diffusion time on diffusivity values was
discovered independently of statistical turbulence theory
while an attempt was being made to extend the work of Conway
(11) to higher flow rates. One method of obtaining a low
noise spin-echo NMR signal with attenuation at normal
gradient for higher flow rates is to operate at shorter
delay times. In preliminary work several different delay
times were used and a wide band of data resulted. When it
was realized that these data were a function of time, a
literature search led to equations such as 17 and 22. The
time range of 4.0 to 10.0 msec diffusion time represented
about the maximum region that the spin-echo equipment could
accommodate up to a Reynolds' number of 7000.

These diffusivity data are presented on Figure 12.
Data were taken at seven different Reynolds' numbers in the
range $3000 < N_{Re} < 7000$. Seven values were considered
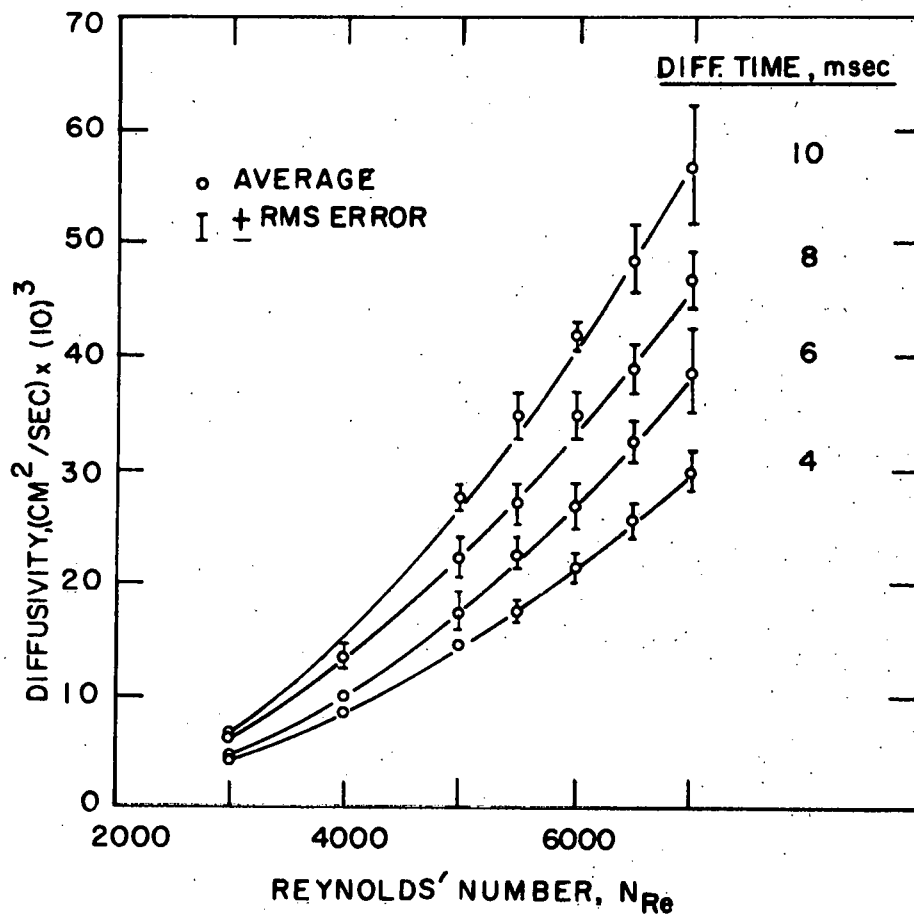adequate since the resultant curve was quite smooth. The

Figure 12.   Diffusivity versus Reynolds' number as a
function of diffusion time

curves shown represent polynomial least squares fits to the data. Each point was replicated four times. The average volumetric diffusivity and the root-mean-square (RMS) error for each diffusion time are given on Table 1 in the Appendix.

The time dependence of the diffusivity data was quite consistent for flow rates above 5000 Reynolds' number. Below this rate, though the data was very reproducible, the time dependence was nonlinear and erratic. This probably resulted because the flow sample was not completely turbulent or the flow profile had not developed. Spin-echo NMR is such a sensitive tool that one can almost "see" flow transition. From oscilloscope observations it appeared that the transition range was much larger than has been reported, with echo fluctuation beginning at about a Reynolds' number of 1800 and not becoming stable until flow reached a Reynolds' number of about 4000.

The data, for $5000 > N_{Re} > 7000$, from Figure 12 were cross plotted as $E(t)$ versus 2τ at fixed Reynolds' number. These points were then fitted by a nonlinear least squares program to Equations 17 and 22. The computer program determined the best values of $\overline{v^2}$ and T_L to fit the data. Figure 13 represents examples of these curves. Neither theoretical equation appears to fit the data adequately, deviating most at the shortest times. Because the Equations 17 and 22 are
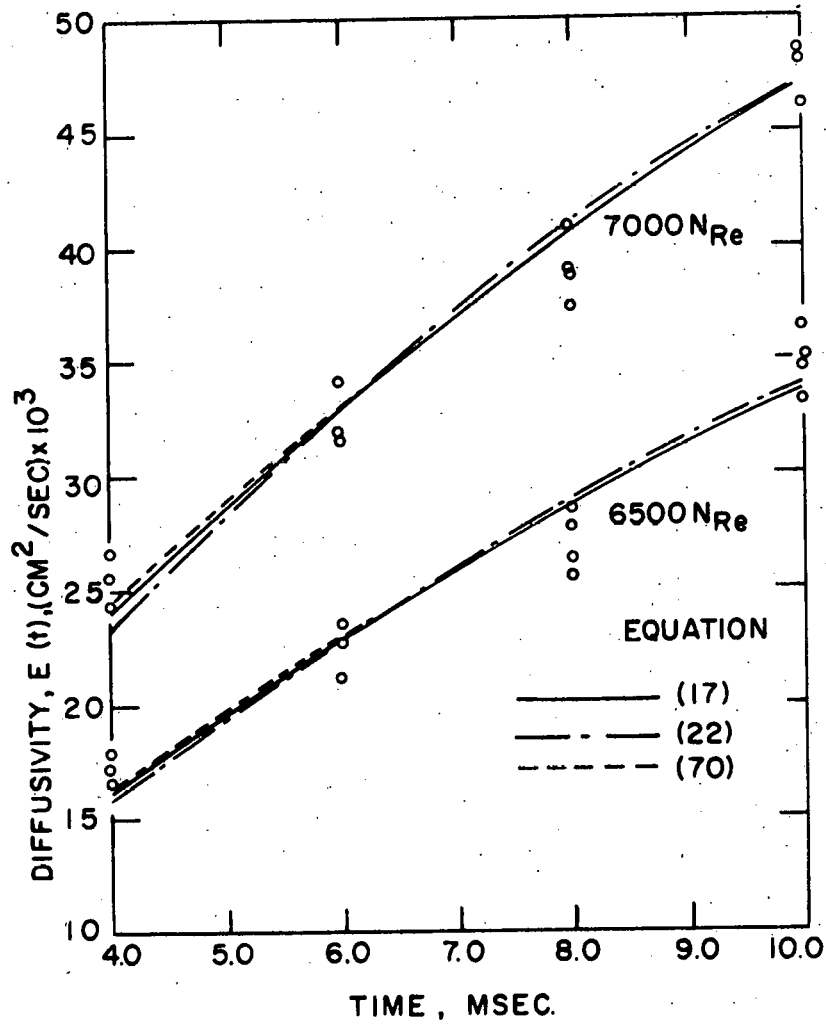
Figure 13. Nonlinear least squares fits to diffusivity data for the assumed correlations

based on assumptions of the shape of the correlation curve, and because there is no comparable data in this time range, the following relation was used to improve the fit at short times. If $R(s) = e^{-as^{1/2}}$ then $T_L = 2/a^2$ or $a = (2/T_L)^{1/2}$. This gives

$$
\begin{aligned}
D = \ & \bar{v}^2 \left[T_L \left[1 - e^{-\left[\frac{2t}{T_L}\right]^{1/2}} \left(\left(\frac{2t}{T_L}\right)^{1/2} - 2 \right) \right] \right. \\
& + 2 \left(\frac{t \, T_L}{2}\right)^{1/2} e^{-\left[\frac{2t}{T_L}\right]^{1/2}} \\
& \left. - \frac{3T_L^2}{t} \left(1 - e^{-\left[\frac{2t}{T_L}\right]^{1/2}} \left(\left(\frac{2t}{T_L}\right)^{1/2} + 1 \right) \right) \right]
\end{aligned}
\tag{70}
$$

The nonlinear least squares fit to this equation is also shown on Figure 13. Although there is only a small difference in the fit of these equations there are signif-icant differences in the values for $\bar{v}^2$ and T_L. Since there are no data in the literature to compare to at these short times one cannot say which, if any, of the relationships is correct. It appears that for this experimental apparatus there was slightly more correlation at very short times than is predicted by the exponential correla-tion decay assumptions. The data are listed in Table 2. While each assumed correlation decay gives consistent results for $\bar{v}^2$, the eddy velocity perpendicular to flow,

overall correlation was not shown to be a function of Reynolds' number. Figure 14 shows a correlation curve for this research which is representative of each of the three theoretical equations. At a Reynolds' number of 5000, turbulence might not be strong enough to satisfy the required isotropic conditions. At a Reynolds' number of 5500 and 6000 the curves are nearly identical, and similarly at 6500 and 7000 another curve is shown. This is evident from the nearly equal values of T_L given in Table 2. The result probably indicates the lack of isotropy in the sample, since there should be a distinct curve for each different Reynolds' number. The assumption of an isotropic sample, at least in the radial direction, which is necessary for mathematical solution of turbulence theory equations, can only be approached in actual experimentation.

Eulerian correlation data similar to Figure 13 were obtained by Martin and Johanson (25). However, they were reporting on longitudinal turbulence fluctuations, which the work of Laufer (24) and Sandborn (33) has shown to be somewhat different than the radial components. Using photographs of hot-film anemometry signals displayed on an oscilloscope, values of voltage versus time were obtained. These data were then computed to determine $\overline{u}(t)$, $\overline{u^2}(t)$, and $\overline{u(t)\,u(t + t')}$ values. The correlation coefficient was calculated directly by Equation 4. These data were in
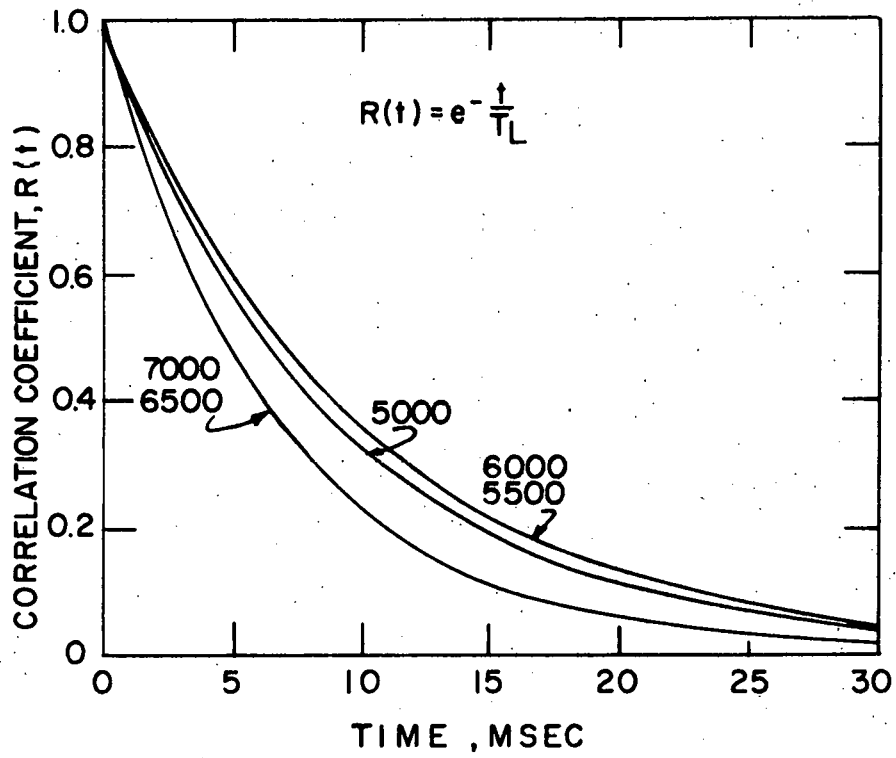
Figure 14. Correlation coefficient, R(t), at different
Reynolds' numbers

a much higher Reynolds' number range because a 6-inch dia.
tube was used, $19,000 < N_{Re} < 160,000$. A consistent
family of correlation curves resulted from this experi-
mentation.

Lagrangian Intensities

The three sets of intensity data given in Table 2, make
it difficult to compare with existing data, but the values
calculated by Equation 17 appear to be in closer agreement
with Eulerian data which has been cited (24, 33). On
comparison of relative radial intensity, as shown in Figure
15, the values obtained by this research are higher than
an extrapolation of the work of Sandborn and also Laufer would
indicate. For relative radial intensities these two investi-
gators were in close agreement. In calculating the relative
values, the maximum velocity at the center of the tube was
not measured in this research. The maximum velocity was
estimated from the average velocity using the data of Senecal
and Rothfus (36). The Lagrangian data of Conway (11) are
also somewhat lower, but it was calculated by Equation 13
which assumes a correlation coefficient of unity. Figure
14 shows that correlation decays even in the short time of
3 msec. If the data were recalculated using Equation 17
higher intensities would result. Both the work of Conway
and the present study, using NMR methods, indicate a slight
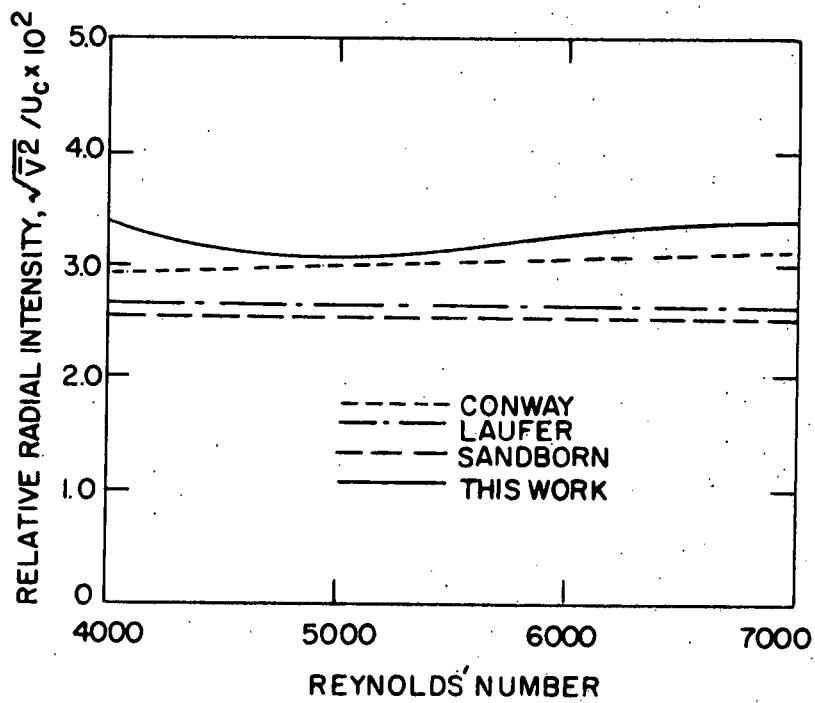decrease in relative intensity as Reynolds' number decreases.

Figure 15. Comparison of turbulent radial intensities with existing data

This is the opposite of research done using anemometry techniques (24,25,33). The change in slope may be the result of shifting from point values in the center of the duct to average values. Measured profiles (25, 33) have shown that the average value is higher than the center value. From this the spin-echo NMR research data could be somewhat higher, as indicated on Figure 15.

Another reason for this trend may be that turbulence is still not fully developed. Only a small flow range has been studied so the question cannot yet be resolved and, at present, spin-echo NMR is limited at about this maximum flow rate, but Hinze (21) states that turbulence is not fully developed below a Reynolds' number of 10,000. The visual observations of NMR signals seem to confirm this idea, if not that specific value.

The agreement between the intensity values obtained in this research and that of Conway, compared to those measured by anemometry methods, confirms that spin-echo NMR can be an effective method for studying turbulence. Further application at higher Reynolds' numbers, with more experimental precautions taken to produce isotropy, should yield more consistent correlation results. These data would either confirm or improve the present theory of statistical turbulence.

CONCLUSIONS AND RECOMMENDATIONS

Conclusions

1. Spin-echo NMR provides a very effective technique for studying fluid turbulence in a pipe. The technique gives a method for statistically following the motion of particles in a fixed volume of fluid. The spin-echo technique has the advantage, when compared to other methods, of rapid, direct measurement without physically or chemically disturbing the flow.

2. The collection of valid diffusivity data as a function of time gives the turbulence parameters, $\overline{v^2}$ and T_L, once a correlation decay shape is assumed. Further work with this technique should clearly distinguish the correct correlation decay shape, then the turbulent flow parameters can be easily determined from diffusivity-time data using nonlinear least squares techniques.

3. Spin-echo NMR is a very sensitive analytical technique, not limited by the response times or frequency sensitivity limitations of many existing methods. With the electronic equipment available, such as the boxcar integrator, signals can be extracted from very noisy outputs.

4. The complete transition range of laminar to fully developed turbulent flow can be ascertained using spin-echo NMR. The induced voltage signal is very erratic

at the critical Reynolds' number, but the transition
and its effect on the data is evident over a much
larger range.

Recommendations

1. Diffusion data at 7000 Reynolds' number should be taken
   to diffusion times as short as possible with the existing
   equipment. These data will be limited by the magnitude
   at which the gradient causes artificial nutation. At
   these short times, T_1 can be decreased to improve the
   time limitation of thermal equilibrium.

2. This study should be extended to much higher Reynolds'
   numbers; i.e., 200,000. To do this will require larger
   pumping equipment and a magnet having larger diameter
   pole faces and a wider air gap. The use of a longer
   axial receiving coil would permit data collection at
   longer diffusion times. It appears that field homoge-
   neity of the existing magnet would allow this.

3. The spin-echo technique can be used to study the flow
   of suspensions or emulsions. By adding nonresonant
   solids to the system, the effect of concentration on
   turbulence could be determined.

NOMENCLATURE

$A(t)$	attenuation function for effects other than diffusion, dimensionless
D	molecular diffusion coefficient, cm^2/sec
d	tube diameter, cm
$E(t)$	turbulent diffusivity, an average over time t, cm^2/sec
G	magnetic field gradient in y-direction, gauss/cm
$\overline{H}_O$	static magnetic vector in y-direction
$\overline{H}_1$	magnetic vector of the rf pulse, 10 MC/sec
$|\overline{H}|$	magnitude of vector $\overline{H}$, gauss
I	gradient coil current, ma
J_1	first order Bessel function
$\overline{L} = d\overline{M}/dt$	torque on the moment $\overline{M}$
$\overline{M}(y)$	summation of the moments in each y-location (x-z plane) at time t
$\overline{M}(t)$	summation of all the moments in the coil at time t
N_{Re}	Reynolds' number
$P(\phi_D)$	distribution in phase of moments across y after time t
$R(s)$	Lagrangian correlation coefficient, dimensionless
T_1	longitudinal, or spin-lattice, relaxation time, sec

T_2 transversal, or spin-spin, relaxation time, sec

t_{90} length of the 90° pulse, sec

t_{180} length of the 180° pulse, sec

T_L Lagrangian time scale of turbulence, sec

$v(t)$ instantaneous turbulent velocity of particles in y-direction, cm/sec

$\overline{v^2}$ Lagrangian turbulence intensity, the mean-square turbulent velocity in the y-direction, cm^2/sec^2

$Y(t)$ distance in y-direction which a particle travelled in time t, cm

$\overline{Y}(t)$ average displacement in y-direction of a large number of particles in time t, cm

$\overline{Y^2}(t)$ mean-square distance travelled in y-direction by particles during time t, cm^2

γ gyromagnetic ratio of nuclei, $gauss^{-1}sec^{-1}$

ϕ phase of each $\overline{M}(y)$ precessing moment

ϕ_o phase of the initial random walk $\overline{M}(y)$ moment at $t = 0$

ϕ_D difference in phase from ϕ_o after time t

τ time duration between the leading edges of the 90° and 180° pulses, sec

2τ total diffusion time, sec

χ magnetic susceptibility of the nuclei

ω_o resonant angular frequency of the center moment, Larmor frequency, sec^{-1}

LITERATURE CITED

1. Abragam, A. The principles of nuclear magnetism. London, England, Oxford. 1961.

2. Andrew, E. R. Nuclear magnetic resonance. Glasgow, England, Cambridge. 1955.

3. Arnold, D. W. Flow measurement by nuclear magnetic resonance techniques. Unpublished M.S. thesis. Ames, Iowa, Library, Iowa State University of Science and Technology. 1963.

4. Batchelor, G. K. Homogeneous turbulence. Glasgow, England, Cambridge. 1953.

5. Bird, R. B., W. E. Stewart, and E. N. Lightfoot. Transport phenomena. New York, N.Y., Wiley. 1960.

6. Bloch, F. Nuclear induction. Phys. Rev. 73:679-712. 1948.

7. Brodkey, R. S. The phenomena of fluid motions. Reading, Mass., Addison-Wesley. 1967.

8. Capps, D. O. and T. R. Rehm. Empirical expression for the turbulent flow velocity distribution. I. and E. C. Proc. Des. and Dev. 7:311-313. 1968.

9. Carr, H. Y. and E. M. Purcell. Effect of diffusion on free precession in nuclear magnetic resonance experiments. Phys. Rev. 94:630-638. 1954.

10. Christiansen, D. E. Turbulent liquid mixing. I. and E. C. Fund. 8:263-271. 1969.

11. Conway, J. E. A study of turbulent diffusion using spin echo NMR techniques. Unpublished Ph.D. thesis. Ames, Iowa, Library, Iowa State University of Science and Technology. 1968.

12. Douglass, D. C. and D. W. McCall. Diffusion in paraffin hydrocarbons. Jour. Phys. Chem. 62:1102-1107. 1958.

13. Flint, D. L., H. Kada, and T. J. Hanratty. Point source turbulent diffusion in a pipe. A. I. Ch. E. Jour. 6: 325-331. 1960.

14. Frantisak, F. A., A. Palade de Iribarne, J. W. Smith, and R. L. Hummel. Nondisturbing tracer technique for quantitative measurements in turbulent flow. I. and E. C. Fund. 8:160-167. 1969.

15. Goldstein, R. J. and W. F. Hagen. Turbulent flow measurements utilizing the Doppler shift of scattered laser radiation. Phys. Fluids 10:1349-1352. 1967.

16. Gordon, S. L. and C. W. Tobias. Unpublished M.S. thesis. Berkeley, California, Library, University of California. 1963.

17. Grossman, L. M. and A. F. Charwat. The measurement of turbulent velocity fluctuations by the method of electromagnetic induction. Rev. Sci. Instr. 23:741-747. 1952.

18. Hahn, E. L. Spin echos. Phys. Rev. 80:580-594. 1950.

19. Hanratty, T. J. Heat transfer through a homogeneous isotropic turbulent field. A. I. Ch. E. Jour. 2:42-45. 1956.

20. Hanratty, T. J., G. Latinen, and R. H. Wilhelm. Turbulent diffusion in particulately fluidized beds of particles. A. I. Ch. E. Jour. 2:372-380. 1956.

21. Hinze, J. O. Turbulence. New York, N.Y., McGraw-Hill. 1959.

22. Johnson, D. C. Apparent radial eddy diffusivities calculated from spin-echo NMR observations. Unpublished M.S. thesis. Ames, Iowa, Library, Iowa State University of Science and Technology. 1966.

23. Knudsen, J. G. and D. L. Katz. Fluid dynamics and heat transfer. New York, N.Y., McGraw-Hill. 1958.

24. Laufer, J. Investigation of turbulent flow in a two-dimensional channel. Nat. Advis. Comm. for Aero. Report TN 1053. 1951.

25. Martin, G. Q. and L. N. Johanson. Turbulence characteristics of liquids in pipe flow. A. I. Ch. E. Jour. 11:29-33. 1965.

26. Mickelson, W. R. An experimental comparison of the Lagrangian Eulerian correlation coefficients in homogeneous isotropic turbulence. Nat. Advis. Comm. for Aero. Tech. Note NACA TN 3750. 1955.

27. Mitchell, J. E. and T. J. Hanratty. A study of turbulence at a wall using an electrochemical wall shear-stress meter. J. Fluid Mech. 26:199-221. 1966.

28. Pake, G. E. Fundamentals of nuclear magnetic resonance absorption. I. Amer. Jour. Phys. 18:438-452. 1950.

29. Patterson, G. K. and J. L. Zakin. Hot-film anemometry measurements of turbulence in pipe flow: organic solvents. A. I. Ch. E. Jour. 13:513-518. 1967.

30. Purcell, E. M. Nuclear magnetism in relation to problems of the liquid and solid states. Science 107:433-440. 1948.

31. Reiss, L. P. and T. J. Hanratty. An experimental study of the unsteady nature of the viscous sublayer. A. I. Ch. E. Jour. 9:154-160. 1963.

32. Reiss, L. P. and T. J. Hanratty. Measurement of instantaneous rates of mass transfer to a small sink on a wall. A. I. Ch. E. Jour. 8:245-247. 1962.

33. Sandborn, V. A. Experimental evaluation of momentum terms in turbulent pipe flow. Nat. Advis. Comm. for Aero. Tech. Note NACA TN 3266. 1953.

34. Schwartz, J. Spin echo apparatus. Rev. Sci. Instr. 28:780-789. 1957.

35. Seagrave, R. C. Mass transfer in liquid streams. Unpublished M.S. thesis. Ames, Iowa, Library, Iowa State University of Science and Technology. 1959.

36. Senecal, V. E. and R. R. Rothfus. Transitional flow of fluids in smooth tubes. Chem. Eng. Prog. 49:533-538. 1953.

37. Sherwood, T. K. and R. L. Pigford. Absorption and extraction. New York, N.Y., McGraw-Hill. 1952.

38. Sirkar, K. K. and T. J. Hanratty. Limiting behavior of the transverse turbulent velocity fluctuations close to a wall. I. and E. C. Fund. 8:189-192. 1969.

39. Tanner, J. E. Pulsed field gradients for NMR spin-echo diffusion measurements. Rev. Sci. Instr. 36: 1086-1087. 1963.

40. Taylor, G. I. Diffusion by continuous movements. London Math. Soc. Proc. 20:196-211. 1921.

41. Taylor, G. I. Statistical theory of turbulence. Royal Soc. (London) Proc. 151A:421-454. 1935.

42. Taylor, G. I. Statistical theory of turbulence. Royal Soc. (London) Proc. 156A:307-325. 1936.

43. Taylor, G. I. and T. Von Karman. Turbulence. Jour. Royal Aeronaut. Soc. 41:1109-1143. 1937.

44. Torrey, H. C. Bloch equations with diffusion terms. Phys. Rev. 104:563-565. 1952.

45. Woessner, D. E. Self-diffusion measurements in liquids by the spin echo technique. Rev. Sci. Instr. 31:1146. 1960.

ACKNOWLEDGMENTS

APPENDIX

Table 1. Diffusivity data as a function of diffusion time

N_{Re}	Avg. E(t) $(cm^2/sec) \times 10^3$	RMS error $(cm^2/sec) \times 10^3$	% RMS error
	$2\tau = 4$ msec		
3000	4.0700	0.2208	5.4247
4000	8.4058	0.6554	7.7973
5000	14.3890	0.4836	3.3606
5500	17.2548	0.9123	5.2874
6000	21.1008	1.4471	6.8583
6500	25.5073	1.5522	6.0855
7000	29.7160	2.0173	6.7888
	$2\tau = 8$ msec		
3000	6.0880	0.9369	15.3894
4000	13.4640	1.3649	10.1375
5000	22.1365	1.8774	8.4808
5500	26.9243	2.2638	8.4081
6000	34.6515	2.3216	6.6998
6500	38.7873	2.5048	6.4578
7000	46.5645	2.8339	6.0859

Avg. E(t) (cm^2/sec) x 10^3	RMS error (cm^2/sec) x 10^3	% RMS error
	2τ = 6 msec	
4.4000	0.6175	14.0331
9.8323	0.3590	3.6513
17.1068	1.8094	10.5772
22.4388	1.6963	7.5598
26.6285	2.1548	8.0921
32.2725	2.1543	6.6753
38.4638	4.2041	10.9300
	2τ = 10 msec	
6.4735	0.3386	5.2308
13.1610	1.3864	10.5343
27.4420	1.1766	4.2875
34.6048	2.3389	6.7588
41.6865	1.2399	2.9743
48.2120	3.4575	7.1714
56.5483	5.8649	10.3716

Table 2. Lagrangian parameters for each assumed correlation shape

N_{Re}	$R = e^{-as}$		$R = e^{-as^2}$		$R = e^{-a(s)^{1/2}}$	
	$\overline{v^2}$ cm^2/sec^2	T_L msec	$\overline{v^2}$ cm^2/sec^2	T_L msec	$\overline{v^2}$ cm^2/sec^2	T_L msec
3000	2.55	4.04	2.01	4.53	3.98	3.63
4000	5.83	3.49	4.62	3.91	9.50	2.84
5000	7.50	9.02	6.54	7.56	9.61	14.91
5500	9.21	9.72	8.12	7.83	11.58	17.38
6000	11.31	9.65	10.04	7.57	14.18	17.53
6500	14.40	6.91	12.22	6.38	19.40	9.45
7000	17.13	6.81	14.59	6.21	23.06	9.30